
Article:
Carey, John J and McKenna, Keith P. orcid.org/0000-0003-0975-3626 (2018) Does Polaronic Self-Trapping Occur at Anatase TiO2 Surfaces? Journal of Physical Chemistry C. 27540–27553. ISSN 1932-7455

https://doi.org/10.1021/acs.jpcc.8b09437

Does Polaronic Self-Trapping Occur at Anatase TiO_2 Surfaces?

John J. Carey* and Keith P. McKenna*

Physics Department, University of York, Heslington, YO10 5DD, York, United Kingdom

E-mail: john.carey@york.ac.uk; keith.mckenna@york.ac.uk

Abstract

The behavior of electron and hole charge carriers at surfaces of titanium dioxide (TiO_2) controls performance for important applications including photocatalysts and solar cells. While anatase TiO_2 exhibits high electron mobility in the bulk a commonly held belief is that strong coupling between electrons and phonons can lead to electron trapping at anatase surfaces. However, direct evidence is scarce and the nature of the trapping sites and electronic properties remains unclear. To address this question we investigate the trapping of electrons and holes at low and high index surfaces of anatase TiO_2 using an accurate hybrid density functional theory approach. We find that, as in the bulk, electrons do not trap on the low index planes (001, 100, 101, 110, 112) of anatase crystals. For the higher index planes (103, 105, 107) that contain structural step defects, we find that electrons do trap at the low coordinated Ti cations present on the steps. The trapping of holes at the surfaces of anatase TiO_2 is a more complicated picture, as the distribution of hole traps is facet dependent. 001 and 100 surfaces, as well as 105 and 107 surfaces which have 001 type terraces, have the strongest affinity to trap holes. Hole trapping for the 101, 110, 112 and 103 surfaces is found to be favoured in the sub surface layers and not at the surface facet. These results provide crucial insights into the behavior of electrons and holes in TiO_2 relevant for applications in

photocatalysis and challenge the common perception that electrons trap at low index surfaces of anatase TiO_2.

Introduction

Titanium dioxide (TiO_2) is a technologically important photocatalyst[1–7] having a range of applications for use in paints,[8,9] gas sensors,[10–12] self cleaning agents,[13,14] pollutants removal,[15,16] water splitting,[17–19] CO_2 reduction,[20–22] electrochromic devices,[23] lithium ion batteries,[24,25] and dye-sensitized solar cells.[26,27] TiO_2 has many different polymorphs but while the rutile phase is the most stable bulk phase,[28] anatase is more catalytically active,[29,30] and is more stable at nano-crystalline sizes,[31] making it more interesting to commercial industries. TiO_2 is extensively studied and has received a lot of attention, for commercial and fundamental studies as it inexpensive, abundant, non toxic, and has a relatively large band gap (3.0-3.2 eV),[32–34] thus having exceptional physical, electronic, photoactive, and electrochemical properties to make it a useful photocatalyst. An important aspect for TiO_2 being a superior photoactive material is the transport of electron and hole charge carriers. The generation of the electron-hole pairs by irradiation and then the transport of these carriers throughout the bulk material to the surface which can initiate reactions with adsorbed molecules, is key to understanding this photoactive material.

The behaviour of the charge carriers is vital to the properties and efficiency of TiO_2 for many applications. Electron and/or hole charge carriers can be introduced into TiO_2 by photo-excitation, doping, or by electrical injection under an external bias. These charge carriers can be trapped at point defects (either intrinsic or extrinsic) which can limit their mobility.[35] In addition, the strong electron-phonon coupling in TiO_2 can lead to polaronic localization of charge carriers even in a defect-free system. Polarons can be either large or small depending on the degree of localization and affect the material's overall quantum efficiency.[36,37] Localization of polarons can affect the transport and chemical properties of

TiO_2 and its ability to carry out photocatalytic reactions at its surfaces. The presence of electron polarons (e^-) in a TiO_2 sample are identified as the reduction of a Ti^{4+} cation to a Ti^{3+} species, and hole polarons (h^+) as the oxidation of a lattice O^{2-} anion to a O^- species, which have been shown to be present in TiO_2 samples by electron para-magnetic resonance spectroscopy,[38–42] photo-luminescence,[43–46] and O_2 photo-desorption studies.[47] The nature and mechanisms by which e^- and h^+ polarons form in TiO_2 and their role in photocatalysis remains uncertain, as polarons can transport through the material potentially trapping at lattice sites in the bulk or at at the surface affecting conductivity, and interacting with surface adsorbed species. The polarons can potentially promote conductivity in the material or affect surface reaction mechanisms, however they can also form carrier recombination centres which are detrimental to photo-conductivity. In particular the surfaces of TiO_2 nano-crystals play a vital role in polaron trapping mechanisms interacting with adsorbates, and the spatial separation of e^- and h^+ polaron carriers to improve the quantum efficiency of TiO_2 by reducing the e^-/h^+ recombination pairs.[48,49]

The shape, size, and exposed facets of anatase TiO_2 have direct implications on the photochemical, photocatalytic and electronic properties, as well as charge separation in nano-crystals or nano-rods of TiO_2, which is attributed to the unique behaviour of preferential charge flow to different surfaces.[48] Anatase TiO_2 crystals are synthesized into tetragonal bi-pyramidal shapes with a large area of exposed thermodynamically stable low energy (101) facets that are capped with smaller areas of higher energy (001) facets. The (100) facet is also found to be particularly reactive for photocatalysis, however it is difficult to achieve exposure of this surface on anatase nano-crystals since the the (101) and (001) surfaces are more stable, but the (100) surface is seen under certain growth and synthesizing conditions.[50,51] The differences in electronic properties and reactivities of the different facets is attributed to the density of low coordinated Ti surface sites, where the most reactive surface has the higher density of five coordinated Ti surface (Ti_{5c}) cations.[2] The (100)/(010) and (001) facets are therefore found to be more reactive than (101) facets as these surfaces have a

higher percentage (100%) of Ti_{5c} than the (101) surface (50%). The photocatalytic activity of anatase TiO_2 nano-particles can be manipulated and tuned by synthesizing different particles with different exposed facets. Each surface has different electronic properties as their band gaps and edges are unique to the structure of the surface, thus having different adsorption edges, affecting their charge carriers and overall displaying different e^-/h^+ behaviours and characteristics.[2,52] The (001) surface has a smaller band gap than the (101) surface, resulting in the adsorption edge having a red shift of 6 nm with respect to the (010) and (101) facets resulting in different electronic properties. Controlling the morphology of different TiO_2 nano-particles to expose certain facets is important in producing highly active TiO_2 nano-crystals; there is a desire to produce particles with only (001)/(010) facets as these are more photoactive than having (101) facets present on the TiO_2 samples.[5,53,54] The (001) surfaces are found to be oxidative facets while the (101) facets are reductive facets; there is a preferential flow of photo-generated holes towards the (001) surface while electrons tend to flow to the (101) facet.[48,55–58] TiO_2 crystals with a mixture of (001) and (101) facets are found to have much lower photo-generated e^-/h^+ recombination rates than crystals with a mixture of (001) and (010) facets. The presence of both (001) and/or (010)/(100) facets (oxidation site), and (101) (reduction site) are suggested to separate the e^-'s and h^+'s leading to lower recombination rates.[56,58–61] Indeed TiO_2 crystals with a combination of (001) and (100) facets show much less photocatalytic activity than when (101) surfaces are present indicating that a mixture is required to maximize charge separation and thus enhance the photocatalysis for applications in solar cells and water splitting.

The electronic properties for each surface must be investigated in order to understand their different behaviours in TiO_2 nano-crystals. Standard density functional theory (DFT) calculations have failed to correctly model excess charges and defects in metal oxides such as TiO_2 due to the inherent self interaction error (SIE) which results in an unrealistic de-localization of charge.[62,63] A Hubbard +U correction or a hybrid DFT approach is needed to overcome SIE, and localize the excess charges, in particular extrinsic/intrinsic defects

and correctly model the electronic structure of TiO_2 in agreement with experimental studies.[64–70] DFT+U calculations, employing a +U value on both Ti $3d$ (+U=4.2 eV) and O $2p$ (+U=5.25 eV) predict that both electron and hole polarons from excess charge will trap in stoichiometric anatase TiO_2 bulk, as well as polarons forming in anatase TiO_2 from defect formation; oxygen vacancies ($V_{\ddot{O}}$) and Ti interstitials ($Ti_i^{\cdots}$) donate electrons to reduce Ti cations while Ti vacancies ($V_{Ti}^{''''}$) and O interstitials (O_i'') form holes.[69] Polaronic hopping mechanism were also investigated by DFT+U calculations ($+U_{Ti3d}$=10 eV), where electron hopping from a Ti^{3+} to a Ti^{4+} cation site has a barrier of 0.09 eV,[71] and a hole hopping barrier of 0.16 eV,[72] indicating that electron transport in bulk anatase is easier than hole hopping. Doping strategies to improve conductive behaviour in bulk anatase TiO_2 modelled by DFT+U also show that small polarons can form reduced Ti^{3+} sites from the inclusion of extrinsic Nb and Ta dopants,[73] where high concentrations of Nb doping in anatase TiO_2 crystals creates shallow donor states in the material tuning the electronic properties from semi-conducting to metallic, thus turning anatase into a transparent conducting oxide.[74,75]

Hybrid DFT calculations using the B3LYP functional have found that both excess electrons and holes self trap to form small polarons as Ti^{3+} and O^- species with energy gains of +0.23 eV and +0.74 eV, respectively in anatase TiO_2, where the unoccupied defect level (h^+) is 1.87 eV above the valence band and the occupied defect level (e^-) is 0.73 eV below the conduction band.[76] The trapping of these polarons is more pronounced at the (101) surface with an electron polaron trapping energy of +0.62 eV and a hole polaron trapping energy of +1.45 eV with both polarons having deeper traps in the band gap; the e^- defect level is 1.00 eV below the CB and the h^+ defect level was 2.30 eV above the VB for the anatase (101) surface. The calculations indicate that the (101) surface is thus more susceptible to polaron trapping than the bulk indicating that it is more likely the polarons will migrate and trap at surface facets in line with EPR measurements.[38,77] The trapping of such polarons at the surfaces will effect the adsorption and interaction of molecules at the anatase surfaces, as previously indicated for polaron trapping at rutile TiO_2 surfaces.[78–80] Not only are small

polarons from excess charges found to trap at the (101) surface, but oxygen vacancy formation and dopant incorporation at the surface also facilitate strong polaron trapping.[81] A detailed combined DFT and experimental study by Setvin *et al.*[82] contests previous DFT+U work, and shows that excess electrons in stoichiometric anatase TiO_2 do not form polarons in the bulk but prefer a free-carrier description, where trapping is only observed near oxygen vacancies or donor dopants such as Nb. Photoemission (ARPES) studies have found that formation of oxygen vacancies in anatase form conducting dispersive metallic states providing contrasting evidence to polaron formation in anatase TiO_2,[83] questioning the nature of conductivity in the material and the conventional view that oxygen vacancies are polaronic in nature with shallow donor levels below the conduction band.[84]

We use hybrid-DFT calculations to model the behaviour of electron and hole polaron trapping at the low index and higher index planes of anatase TiO_2. Our work on the anatase surfaces follows on from previous work on the polaron trapping in bulk anatase TiO_2,[85] where we determined the proportion of Hartree-Fock exact exchange based on the Koopmans' condition. The behaviour of electrons and holes at the low index surfaces was found to be similar to the anatase bulk; a delocalised (carrier-free) description of the electron across multiple Ti sites was found to be preferred over a localized polaron solution on one Ti cation, while the holes were found to preferential trap at all surfaces. The introduction of lower coordinated Ti cations at surface steps on higher index planes were found to trap electron polarons indicating that surface defects on nano-crystals of anatase TiO_2 will reduce electron mobility.

Computational Methodology

All calculations were performed using hybrid density functional theory (DFT) and the generalized gradient approximation (GGA).[86] Exact Hartree-Fock (HF) exchange is mixed in to the exchange-correlation function (hybrid-DFT) to overcome the issue of the self-interaction

error (SIE) that is well known in DFT. The hybrid-DFT exchange-correlation functional that is used is referred to as PBE0-TC-LRC which is a truncation method that defines a range of separations in the electron integrals to implement the HF exact exchange, while standard PBE is used outside of this range. The truncation radius must be smaller than half the distance of the lattice vectors to ensure that there is no interaction between neighbouring cells. In our case, we find that setting the truncation radius to 6.00Å is sufficient to correctly describe the electronic properties of the anatase bulk and surfaces. The percentage of HF exact exchange to include in these calculations was parameterized by satisfying Koopmans' condition to within 0.05 eV on bulk TiO_2 anatase, by varying the α value with respect to the eigenenergy. The α value was found to be 10.5% and a detailed description of the approach to achieve this value is described in depth for different polymorphs of TiO_2 in our previous work.[85]

We use a triple ζ basis sets for both Titanium and Oxygen for accurate calculations which are optimized from molecular calculations (MOLOPT),[87,88] and the Goedecker-Teter-Hutter (GTH) pseudopotentials for both species available within CP2K.[89–91] The 'QUICKSTEP' approach for DFT calculations in CP2K is implemented, which uses a multi-grid system for mapping products of Gaussians onto a real-space integration grid. The wide and smooth Gaussian functions are mapped onto a coarser grid, where the electron density is mapped onto the finest grid. The plane wave energy cut-off, a reference grid which controls the Gaussian mapping onto the multi-grid, is set to 60 Ry. Five multi-grids are used, and the plane wave cut-off is sufficiently converged at 600 Ry for the finest level of the multi-grid.

CP2K only uses Γ-point sampling of the Brillouin zone instead of the k-point grids used in typical DFT codes, and we have to use sufficiently large supercells to ensure appropriate sampling of the Brillouin zone. The cell was expanded to a 5x5x2 $Ti_{200}O_{400}$ supercell to ensure that properties were sufficiently converged. The optimized anatase bulk unit cell has lattice vectors $a = b = 3.796$Å and $c = 9.605$ which are within 1% of the room temperature measured experimental lattice vectors.[92] The large system size not only allows accurate

calculations at the Γ point, but also ensures there is a very small interaction between defects in neighbouring image cells from the periodic boundary conditions (PBCs). The electronic structure is efficiently minimized using a 'Full-all' pre-conditioner with a small energy gap (0.01 eV), and the 'Direct inversion in the iterative subspace' (DIIS) algorithm to $1x10^{-6}$ Ry. The ions are relaxed using a BFGS optimizer and are deemed converged when the forces on the atoms are relaxed to less than $4x10^{-4}$ Ry.

The advantage of our method is that limiting the region of HF exact exchange by truncation greatly reduces the computational cost and allows an investigation to be carried out on much larger systems (500-700 atoms) than previously accessible by hybrid-DFT methods. To further improve the efficiency of these calculations, we used the auxiliary augmented matrix method (ADMM) in CP2K, which approximates the exchange integrals for the HF region by mapping the orbitals onto smaller basis sets.[93] The ADMM basis sets of choice are the so called 'FIT3' for Ti and 'pFIT3' for O, which provide a accurate description of the electronic structure as outlined in ref.[85]

The anatase TiO_2 low index surfaces of interest are the (001), (100), (101) and (110) as these are the most theromdynamically stable surfaces and will be more expressed on anatase nano-crystals. The (111) surface is the least stable and not widely expressed on anatase crystals so it will not be examined in this study. The surfaces are generated from the Ti_4O_8 unit cell using the METADISE code,[94] and are modelled using the slab approach. The slab thickness was converged with respect to the surface energy to ensure it is sufficiently thick to have bulk-like properties in the middle of the slab, while demonstrating surface properties at the edge. The stoichiometric surfaces have slab thickness between 24-25 Å with surface areas between 200-300 $Å^2$ and a vacuum gap of 12 Å.

Both electron and hole polarons are modelled in each surface slab by initially moving atoms that are within a 2.2 Å radius of the polaron site, 0.2 Å away from the site, forcing a distortion in the lattice, and then the full geometry relaxation of the slab is carried out. This initial distortion creates a potential well for localization of a polaron on a given lattice site.

The polaron trapping energy is calculated in each surface slab by the following equation;

$$E[\text{trap}] = \text{E[surf]} - \text{E[bulk]} \tag{1}$$

where E[trap] is the calculated trapping energy, E[surf] is the energy of the polaron at the surface site and E[bulk] is the energy of a polaron in the 'bulk-like' region (middle) of the slab. The lattice site as the reference polaron in the 'bulk-like' region of the slab is selected by the ion which most closely resembles the electronic properties of the polaron in the anatase bulk. We examined two approaches to investigate polaron formation; 1) at one side of the slab and 2) on both sides of the slab. The difference in the polaron trapping energy between the two approaches is negligible, so we will investigate polaron trapping on one side of the slab to ease computational efforts. The electronic properties of the polaron in each surface will be detailed by partial (l and n quantum number decomposed) electronic density of states (PDOS), geometric strain, occupation and electron spin, as well as looking at the relaxation of ions in each slab.

Results

Bulk and surface properties

The local geometry for the optimized anatase bulk and the calculated PDOS plot is shown in Figure 1. The figure shows that the Ti^{4+} cations have octahedral geometry with coordination of 6, and the O^{2-} anions have a trigonal planar geometry with a coordination of 3. The bulk Ti^{4+} cations have two 1.99 Å bonds along the c vector and four 1.94 Å bonds in the ab plane. The O^{2-} anions have one 1.99 Å bond along the z vector and two 1.94 Å bonds in the ab plane. The bond angles between all Ti and O atoms is around 102^o. The calculated PDOS for the anatase TiO_2 bulk (Figure 1) shows that the valence band (VB) is dominated by O $2p$ states with some mixing from Ti $3d$ states and minor contributions from the Ti

$3s/p$ states, while the conduction band (CB) is dominated by Ti $3d$ states and some minor mixing from O $2p$ states. The calculated fundamental band gap from VB maximum (VBM) to the CB minimum (CBM) is 3.03 eV, which is in good agreement (<6%) with the anatase experimental band gap measured by photo-luminescence spectroscopy (3.21 eV).[44,46] Our calculated band gap is in better agreement with the experimental band gap than previous DFT+U work and the B3LYP functional, while being in a similar range to other works using the HSE functional. The calculated value has not been fitted to the experimental band gap, and is a result of our choice of HF exact exchange that satisfies Koopman's condition, in turn providing a good description of the electronic properties of bulk anatase TiO_2 which will be implemented for the surfaces.

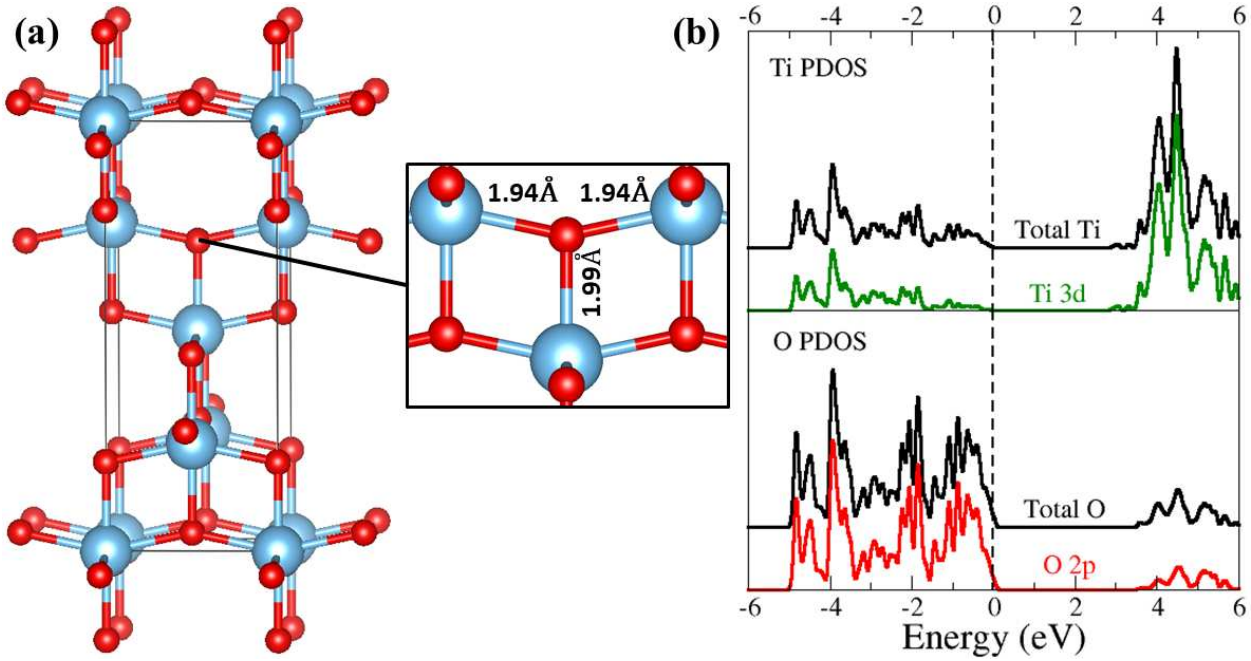

Figure 1: (a) The unit cell and local geometry of the optimized bulk anatase TiO_2, and (b) the calculated PDOS. The blue and red spheres are the lattice sites for the Ti cations and O anions, while the blue, red and green lines are the s, p and d projected DOS respectively.

The structures for the low index anatase TiO_2 surfaces are shown in Figure 2 (a) - (f), which also includes the reconstructed 001 (figure 2 (b)) surface since this is important for catalytic applications of TiO_2 nano-crystals.[54,95] All surfaces are terminated with both Ti cations and O anions, where the Ti cations are five coordinated (Ti_{5c}) and the O anions

are two coordinated (O_{2c}). The higher index planes of anatase TiO_2 (Figure 2 (g)-(i)) are also of interest since anatase nano-crystals/nano-rods are not perfect crystals entirely made of flat low index facets, and many will have surface defects such as steps and kinks. The chosen higher index surfaces, namely the 103, 105 and 107 facets are shown in Figure 2. The structure of the 103 surface shows that it is terminated by rows of four coordinated Ti and two coordinated O species (Ti_{4c} and O_{2c}) , while the 105 surface is terminated by a mixture of Ti_{4c}, Ti_{5c} and O_{2c} species. The 107 surface is similar to the low index planes being terminated by both Ti_{5c} and O_{2c} species.

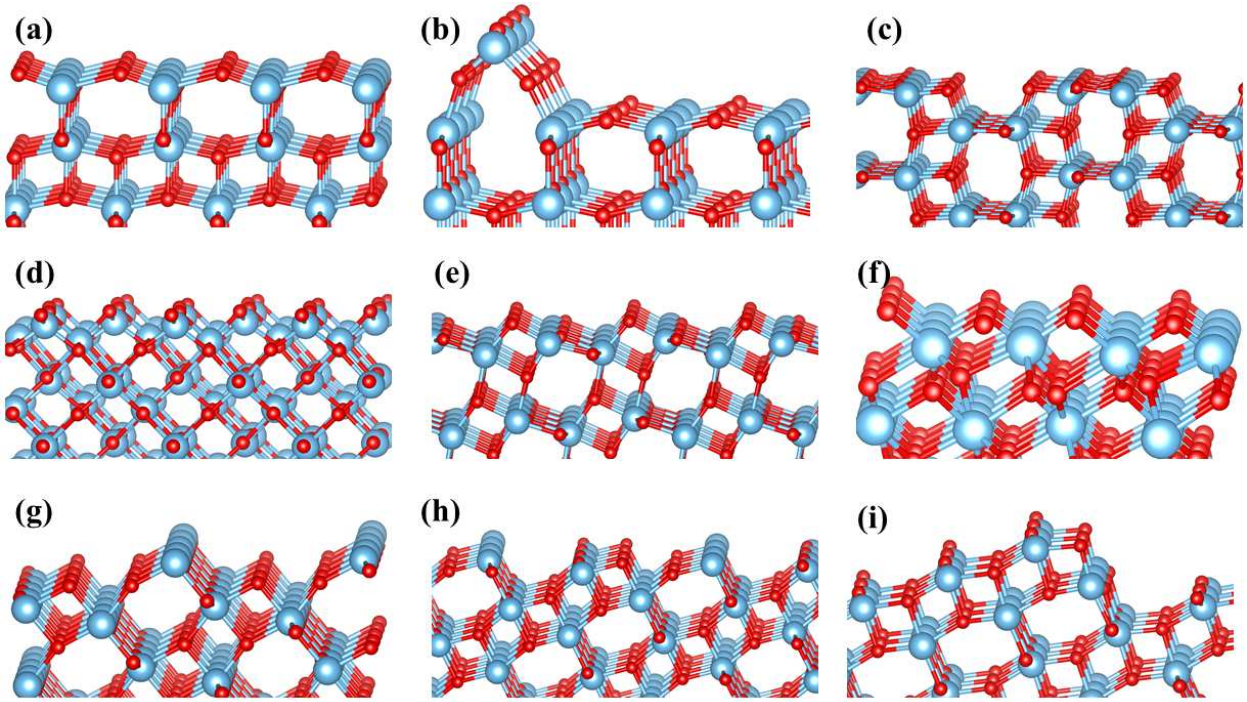

Figure 2: The surface structures of the (a) 001, (b) 001-reconstructed, (c) 100, (d) 110, (e) 101, (f) 112, (g) 103, (h) 105, and (i) 107 low and high index planes of anatase TiO_2. The blue and red spheres are the Ti cations and O anions.

The expansion, area and thickness of the surface slabs, along with the calculated surface energies for each facet are given in Table 1. The slabs are sufficiently large to accommodate polaron formation without negligible interaction between neighbouring images, and they are sufficiently thick to ensure there is little interaction between the surfaces above and below, and to ensure that there is a bulk like region in the slab centre as shown in Figure 3. The

calculated surface energies are similar to previous DFT PBE works,[54,96] and show that the reconstructed (001), (100), (101) and (112) surfaces are the most stable, while the stepped surfaces are higher in energy, as expected, and hence more reactive. A Wulff construction of an anatase TiO_2 nanoparticle using the calculated surface energies (see supporting information; Figure S1 (a)) indicates that an ideal particle would be capped with (001) facets, and has a higher surface area of (101) facets which are joined by (112) facets at the crystal edges. If the surfaces become more stable by 10-20% through synthesis techniques or in the presence of solvents, then we find that the anatase crystals will change shape as 103 surfaces will be exposed on the edge between the 001/101 facets, and in some instance the 103 facet will replace the 001 facet capping the crystals (Figure S1 (b)).

Table 1: The periodicity, stoichiometry, area, thickness and surface energy (γ) for each surface slab.

Facet	Periodicity	Stoichiometry	Area (Å^2)	Thickness (Å)	γ (J/m^2)
001	(4x4)	$Ti_{160}O_{320}$	237.3	22.4	0.99
001-recon	(4x1)	$Ti_{200}O_{400}$	237.3	33.6	0.59
100	(4x2)	$Ti_{208}O_{416}$	296.3	23.1	0.56
110	(2x3)	$Ti_{228}O_{456}$	314.3	24.2	0.97
101	(4x2)	$Ti_{224}O_{448}$	319.1	23.9	0.46
112	(4x1)	$Ti_{176}O_{352}$	268.5	25.6	0.58
103	(5x1)	$Ti_{160}O_{320}$	289.2	20.1	0.97
105	(4x1)	$Ti_{192}O_{384}$	331.1	19.6	1.07
107	(1x3)	$Ti_{168}O_{336}$	330.2	20.5	1.01

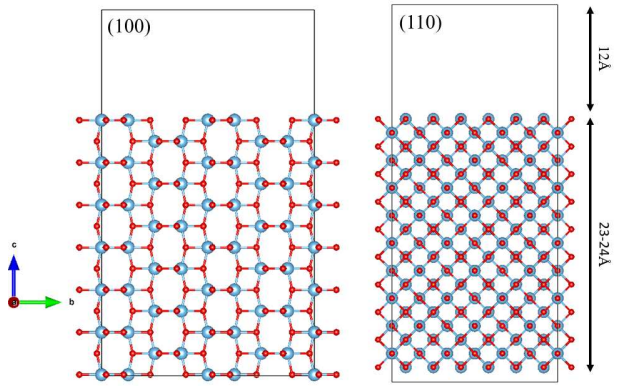

Figure 3: The unit cell of the (100) and (110) surfaces along the a-vector, where the thickness of the vacuum gap and slab thickness are indicated.

The geometric convergence of these surfaces is non-uniform and experience Peierls stress type relaxation,[97–100] which is found to be significant at the surface and also deep into the thick surface slabs. This type of relaxation allows rows of atoms to relax in alternating directions to compensate opposing forces on each row to reach their minimum energy. Examples for the 100, 101 and 110 facets are given in the supporting information (Figure S2-S4) to show that relaxation of the atoms is more pronounced along certain directions, and the direction which we observe the Peierls stress is facet dependent; we do not see the resulting stress in one direction for all surfaces. The effect of the relaxation into the middle of the slab (bulk like region) suggests that this physical disturbance can be observed to at least a depth of 10-13Å in nano-crystals of TiO_2; however we can not investigate if this propagation extends further into crystals of TiO_2 until a bulk-like region with smaller relaxations/forces is reached due to computational limitations. The overall magnitude of the displacement/relaxation is 0.0 for the bulk region (middle) of the slab, while this displacement is greater at the surface edge. We believe this type of relaxation has not been observed before for DFT calculations since previous works have used much smaller slabs, while our surface slabs are sufficiently large enough to describe this behaviour.

The slabs are large enough to accommodate a bulk region of 6-8Å thick in the middle of the slab and a surface region around 6Å thick. The calculated percentage change for the relaxed surface and bulk region bond lengths compared to the bulk TiO_2 crystal are given in Table 2, where the lowest and highest change in the range are associated with the smallest and largest Ti-O bond lengths for a given atom. The table indicates that the surface bonds undergo a considerable relaxation compared to the bonds in the bulk region (middle) of the slab as expected. For the (001) surface, the reconstructed surface has lesser relaxation of the bond lengths than the unreconstructed surface providing an explanation to the decrease in surface energy as seen in Table 1. The surface bond lengths of the (110) and (103) surfaces are all shorter than their bulk counterparts, while the largest relaxations are seen for the (105) and (107) stepped surfaces in line with the largest surface energies (Table

1). All the surface slabs have relaxation that propagates into the bulk region (middle) of the slab, leading to a change of 1% in their bond lengths; however we have seen that the overall magnitude of the atomic displacement in the bulk region is 0.0 from the plots in Figure S2-S4. Although we expect the bond lengths in this region of the slab to be similar to the bulk bond lengths with little relaxation, a change of less than ± 1% in each slab is small enough to say that these atoms can be considered to be bulk-like and used as reference points for calculating the electron/hole trapping energy for each surface.

Table 2: The percentage change for the relaxed bond lengths in the surface and bulk regions for each surface slab facet compared to bulk anatase TiO_2.

Facet	Surface Region (%)	Bulk Region (%)
001	(±) 12	(±) 1
001-recon	(±) 8	(±) 1
100	(±) 7	(±) 1
110	(-) 8	(±) 1
101	(±) 6	(±) 1
112	(±) 9	(±) 1
103	(-) 10	(±) 1
105	(±) 11	(-) 1
107	(±) 12	(±) 1

The calculated PDOS plots for the Ti/O bulk/surface region states for each surface facet are shown in Figure 4. All PDOS plots show that regardless of the surface facet, the bulk and surface region band gaps are similar (around 3 eV) to the anatase bulk band gap. The (001) and (001)-recon PDOS plots have similar characteristics, where the Ti states for the bulk and surface regions are similar; however for the O $2p$ states the surface states lie above the bulk region states by 0.6 eV at the top of the valence band, which can explain the previously observed experimental UV-vis red shift on the (001) surface with respect to other anatase surfaces.[2,52] The PDOS plots for the (100), (101), and (110) surfaces are similar so only the (101) surface is shown in Figure 4. The PDOS plot for the (101) surface shows that there are no special Ti/O surface states and that the bulk and surface regions are similar. For the 103 surface, the bulk O $2p$ states lie above the surface states by 0.2 eV at the top of the valence band (Figure 4 (b)), while there are surface Ti $3d$ states peaks that lie 0.4 eV

below the Ti $3d$ states in the conduction band (Figure 4 (a)). The 105 and 107 PDOS plots show similar features so only the 105 surface is shown in Figure 4. Both surfaces have O $2p$ surface states lying at the top of the valence band, and Ti $3d$ surface states lying at the bottom of the conduction band, above and below the bulk region states. The appearance of the surfaces state peaks and features either at the top of the valence band or the bottom of the conduction not observed for the bulk indicate that the surfaces are expected to show different properties for polaron trapping.

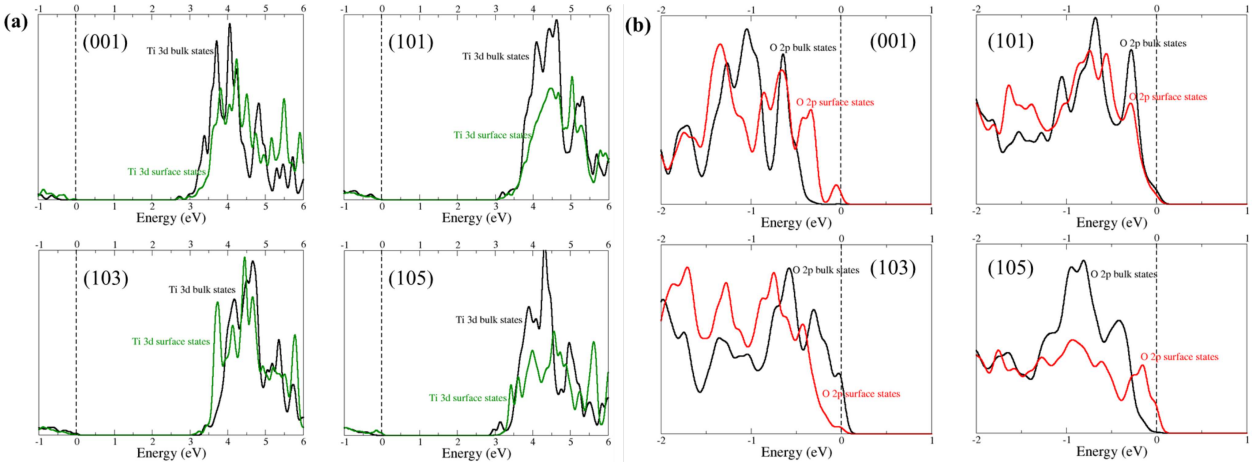

Figure 4: The PDOS of the (a) O 2p and (b) Ti 3d bulk/surface states for the 001, 101, 103, and 105 surfaces of anatase TiO_2. The green and red lines are the Ti $3d$ and O $2p$ states, where the dotted black line indicates the position of the Fermi level.

Electron trapping at anatase surfaces

The presence of excess electrons at the low and high index surfaces of anatase TiO_2 was investigated by adding an extra electron to a Ti^{4+} cation site in the model slab. Ti^{4+} cations in each atomic layer from the bulk region up to the surface sites were investigated for electron trapping. The specific Ti site of interest was first distorted by elongating the Ti-O bonds by 0.2 Å and the surface slab was relaxed at 25% HF exchange to localize the excess electron on the Ti cation forming a Ti^{3+}. As we have previously shown in our work on electron/hole trapping in bulk anatase,[85] this level of HF exchange does not obey Koopman's condition and in order to satisfy this we must then run the localized electron in the surface slab at

10.5% HF exchange. The surface slab with the localized electron charge on the Ti^{3+} cation site is then relaxed with 10.5% HF exchange. For this level of HF exchange, the localized electron charge prefers to become a delocalised solution across multiple Ti cations in the bulk region of all surface slabs. For the low index surfaces, all surface and subsurface sites relaxed to a delocalised electron charge across multiple sites in a similar manner to the bulk like properties of anatase TiO_2. The preference for the delocalised solution across multiple Ti cations supports the carrier-free description of electrons in TiO_2,[82] as opposed to the localized polaron formation previously predicted by DFT+U and hybrid-DFT.[64,81,101] This result indicates that the ideal perfectly flat low index surfaces for the anatase TiO_2 crystals will not trap excess electron charge in either their bulk or surface regions. For the higher index planes that contain steps and low coordinated Ti_{4c} cations, we find that these sites will trap excess electronic charge as the Ti cations remain Ti^{3+} species with localized charge at the 10.5% level of HF exchange as shown in Figure 5. We find that for the 105 and 107 facets, both the Ti_{5c} and Ti_{4c} cations on the steps trap electrons where the Ti_{4c} cations have a lower trapping energy. For all stepped surfaces, the bond lengths for the reduced Ti cation site with the trapped electron elongate by 5-10%.

On closer inspection of the localized electron charge shown in Figure 6, the excess electron preferentially occupies the d_{zy} type orbital for the 103 and 105 surfaces, while for the 107 surface we see charge localized in a d_{z^2} orbital which breaks a Ti-O surface bond to achieve the lower coordinated Ti_{4c} cation similar to the 103 and 105 surfaces that localizes charge. The calculated PDOS in Figure 6 shows that a defect level appears off the bottom of the conduction band at around 0.70 eV, 0.97 eV and 0.96 eV for the 103, 105 and 107 surfaces respectively. These defect peaks are attributed to the electron trapped on a Ti cation, and can be associated with the stepped surface state peak features at the bottom of the conduction band seen in Figure 4. These Ti $3d$ states at the bottom of the conduction band associated with the lower coordinated Ti cations on the step that give rise to electron trapping, are not present for the bulk and low index surfaces which may provide an insight

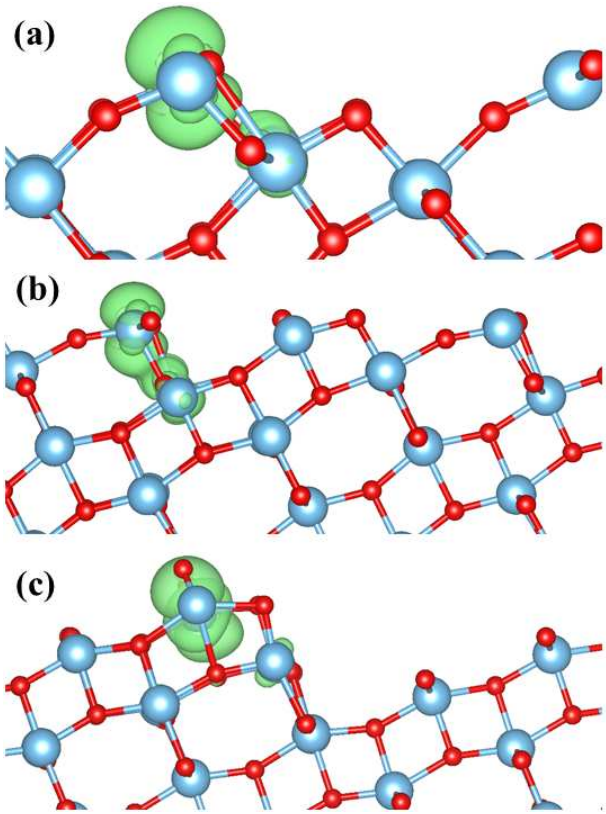

Figure 5: The local geometry (along the a-vector) for electron trapping at the (a) 103, (b) 105 and (c) 107 surfaces of anatase TiO_2. The green iso-surface (0.0015 electrons/$a_o{}^{-3}$) shows the location of the trapped electron at the step.

into the absence of electron trapping.

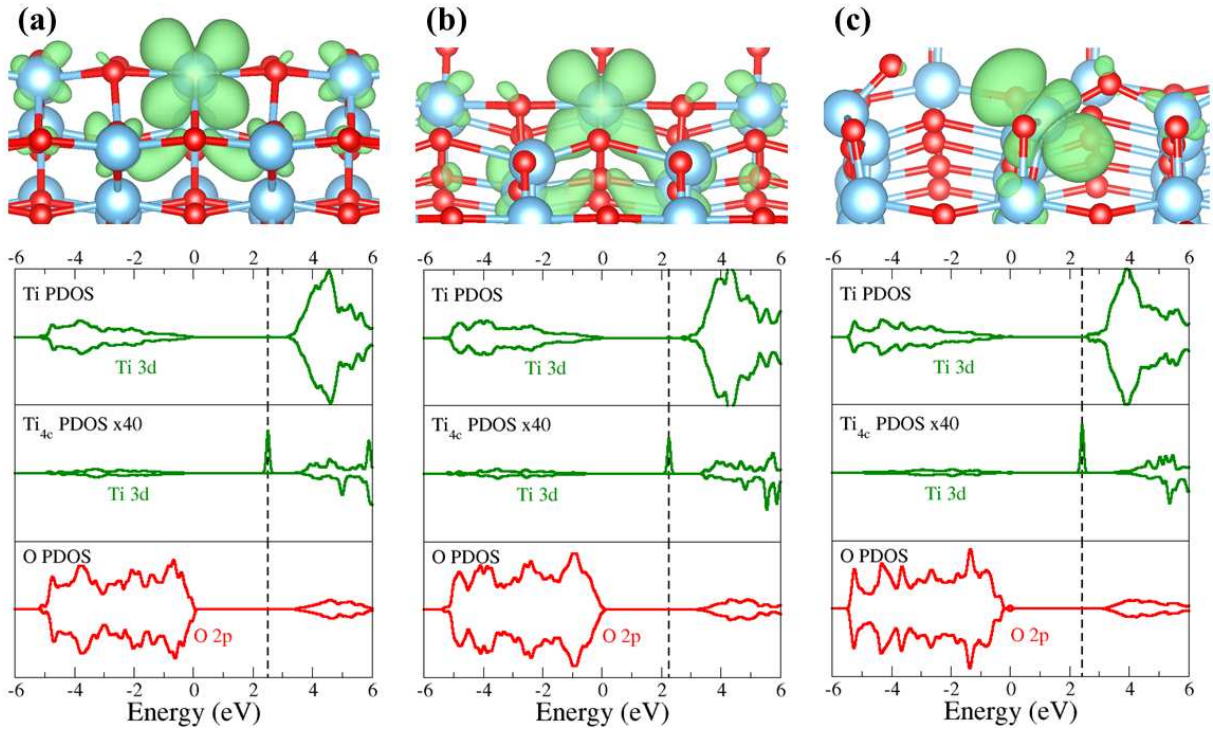

Figure 6: The local geometry (along the b-vector) and PDOS of the electron trapped at the (a) 103, (b) 105, and (c) 107 surfaces of anatase TiO_2. The green iso-surface ($0.0015\,\text{electrons}/\text{a}_o{}^{-3}$) shows the location of the trapped electron polaron, while the green and red lines are the Ti $3d$ and O $2p$ states, where the dotted black line indicates the position of the Fermi level.

The calculated electron trapping energy (E[trap]), position of the defect level from the bottom of the conduction band (E[level]), the strain energy and electron spin for the stepped surfaces are given in Table 3. Since no electron trapping is observed in the bulk like region of the slab, or in the anatase bulk system, we have to calculate the electron trapping energy in the stepped surface with reference to the energy cost to go from a localized state to a delocalised state in bulk anatase. A positive electron trapping energy for all stepped surfaces indicates that the electron surface trap is less energetically favourable to form than the delocalised solution in the bulk. This indicates that electrons are more likely to remain in a delocalised state in the anatase bulk than trap at surface defect sites like steps. The excess electron trapping at the surface step site would suggest that its a kinetic trap, and

that energy supplied to the anatase surface to overcome the trap will allow electrons to move favourable back into the bulk. The deep defect levels from the electron trap around 1 eV below the conduction band indicates the energy required to excite the electron back into the conduction band. The calculated strain energy, which is the energy to distort the lattice site in order to trap charge, indicates that the energy to form the trap is higher than the electron trapping energy, where the largest localization shown by the spin is associated with the strongest trap on the 107 surface. These results show that electron trapping of excess electrons in anatase crystals will occur when surface structural defects such as steps, and kinks are present.

Table 3: The calculated electron trapping energy, defect level, strain energy, and spin for the most favourable configuration in each of the surface slabs.

Facet	E[trap] (eV)	E[level] (eV)	Strain (eV)	Spin (μ_B)
103	+0.07	0.70	1.05	0.73
105	+0.17	0.97	0.97	0.61
107	+0.58	0.96	1.25	0.89

Hole trapping at anatase surfaces

The trapping of single hole and hole bi-polarons at the rutile and anatase TiO_2 surfaces, and indeed other metal oxides, is important for catalytic purposes, as these holes may diffuse to the surfaces, interacting with molecular species.[102,103] This work focuses on single hole trapping at the oxygen sites in the low and high index surfaces of anatase crystals, which is examined by removing an electron, and creating a hole state at a specific lattice O site. This is carried out in a similar way to examining excess electron trapping, where the energy to form a hole polaron in the surface slab is calculated at specific O sites in the bulk region of the slab all the way to the surface region as shown by some examples in Figure 7. The O lattice site is initially distorted by elongating the Ti-O bonds around the site by 0.2 Å and the electron is removed from the lattice O creating the hole polaron. The slab is initially relaxed with 25% HF exchange to localize the charge, and then further relaxed at our generated HF

exchange alpha value of 10.5%.

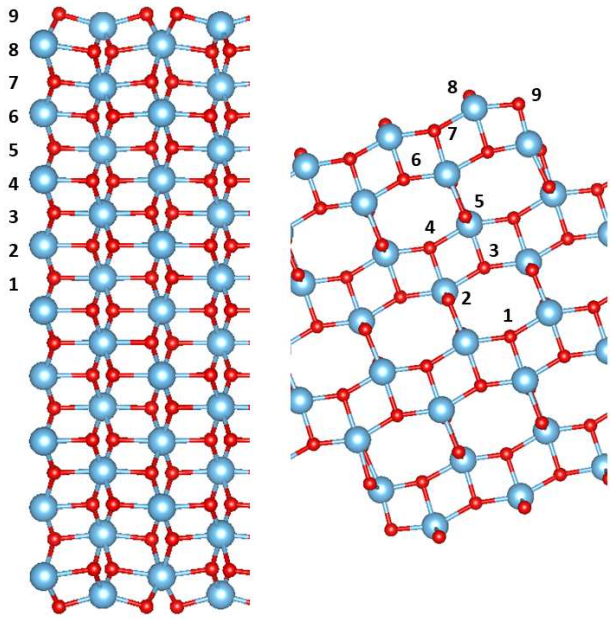

Figure 7: Examples of a low and high index surface slabs with the sites from the bulk to the surface region labelled to examine hole trapping.

The O surface sites labelled in Figure 7 are associated with the calculated hole trapping energies provided in Table 4. Hole trapping is stable at all O sites from the bulk to the surface region. The calculated hole trapping energies from the middle of the slab up to the first 4 atomic levels can be considered the bulk region as a reference point since they have similar energies, all are within $< 0.1\,\text{eV}$. The bond distances for the relaxed hole polaron in the middle of the slabs are within $\pm 2\%$ of the bond distances for the hole polaron in bulk anatase. The good agreement between the hole polaron in the middle of the slabs and the bulk indicates that the hole polarons are similar and can be used as a reference point to calculate the hole trapping energy in the surface layers. The omitted values in Table 4 for certain layers of different facets indicates that the hole trap was not stable at this point. The distribution for hole trapping energies in the top surface layers is different for each surface facet; the 001 surface, 001 reconstructed, 105 and 107 surfaces have strong hole trapping at their surface edges, while the other surfaces have less favoured hole trapping at the surface. The 105 and 107 stepped surfaces have strong trapping energies as the flat

terrace perpendicular to the step is a 001 type facet. The 100 surface has meta-stable traps across a number of atomic layers, where the sub-surface layer has the most favoured hole trapping energy. Hole trapping in the 101 facet is favoured across a number of layers below the surface, whole the 110 surface has favoured trapping in the sub-surface layer but also has a meta-stable hole trapped at the surface. For the 112 and 103 surfaces the hole trapping close to the surface is unfavourable compared to the bulk, and there are meta-stable hole traps a number of layers below the surface.

Table 4: The calculated hole trapping energy from the bulk to the surface regions in each of the surface slabs. All values are referenced to the formation of a hole in the middle layer of the slab and are in eV.

Facet	1	2	3	4	5	6	7	8	9
001	0.00	0.00	0.00	0.01	0.06	-	-	-	-1.13
001-recon	0.00	0.00	0.00	0.01	0.09	-	-	-0.16	-1.17
100	0.00	0.00	0.05	0.03	0.19	-0.05	0.02	-0.12	0.07
101	0.00	-0.09	0.05	-0.06	0.17	-0.15	-0.06	-0.06	0.30
110	0.00	-0.08	-0.08	-0.08	0.07	-0.11	0.20	-0.18	-0.02
112	0.00	0.00	0.00	0.00	0.04	-0.06	0.06	0.06	0.13
103	0.00	0.00	0.00	0.08	0.07	-0.04	0.26	0.10	0.21
105	0.00	0.00	0.03	-0.09	-0.11	-	-	-	-1.37
107	0.00	0.00	0.00	0.03	-0.09	0.13	-0.75	-0.83	-0.75

The hole trapping energy, defect level, strain energy and hole spin for the most favoured trapping sites on each of the surfaces is given in Table 5. The table shows that the 001, 105 and 107 surfaces have the strongest trapping energies, while the 103 and 112 have the least favoured trapping energies. The 100 , 101 and 110 surfaces have similar trapping energies. There does not appear to be a correlation between trapping energies and the position of the defect level; however if we examine the PDOS plots in Figure 4 there are O $2p$ surface peak features at the top of the valence band for the 001/001-recon, 105/107 surfaces that are not present for the 100/101/110 and 103/112 surfaces. These states at the top of the valence band are more easily depopulated giving rise to the more strong hole trapping energies and in some cases having deeper defect levels. Again for the strain energy there is no direct trend/correlation for the hole trapping energy and strain energy; however there appears

to be in most cases, a smaller energy required to create the lattice distortion to localize the charge associated with the strongest hole trapping energy, while the facets with lower trapping energies have a larger strain energy. The stronger hole traps have between 8-14% more localized charge than the surfaces with the weaker traps which have more dispersed charge around the trap site.

Table 5: The calculated hole trapping energy, defect level, strain energy, and spin for the most favourable configuration in each of the surface slabs.

Facet	E[trap] (eV)	E[level] (eV)	Strain (eV)	Spin (μ_B)
001	-1.13	2.32	1.30	0.85
001-recon	-1.17	1.98	1.20	0.89
100	-0.12	0.90	1.57	0.76
101	-0.15	1.40	1.34	0.77
110	-0.18	1.56	1.44	0.76
112	-0.06	2.66	1.36	0.75
103	-0.05	2.16	1.25	0.78
105	-1.37	2.10	1.12	0.87
107	-0.83	2.05	1.71	0.89

The calculated spin density and PDOS for the most favoured hole trapping sites (Table 5) in each of the surface facets are shown in Figures 8 and 9. Hole trapping at all surfaces has *p*-like character along different directions for each facet. For the 001 surfaces the presence of a hole on the surface breaks a Ti-O bond resulting in low coordinated surface $O^{-}{}_{1c}$ species where the charge is very localized on the 001 surface. The position of the hole trap on the 100 is on the lower coordinated surface O_{2c} rather than the surface O_{3c} species, where the charge is distributed across a number of surface and sub-surface O anions. For the 110, 101 and 112 facets, the hole trap is in the sub-sub surface layer distributed across a number of lattice O sites, which is also seen for the stepped 103 surface in Figure 9. The position of the hole trap is on the 001 terrace of the 105 and 107 facets, where a Ti-O bond is broken to accommodate the hole trap in a similar manner to the 001 surface that is not observed on the 107 surface. This may explain the stronger hole trapping energy for the 105 surface over the 107 surface. Although the distribution of hole trapping energies in Table 4 shows that the hole trapping is favoured across multiple sites and the step on these facets indicating

that they are strong hole trapping surfaces.

Discussion

The hybrid-DFT approach we implement (PBE0-TC-LRC) using 10.5% HF exact exchange provides invaluable insights into the polaron trapping properties of anatase low and high index surfaces. The value of HF exact exchange has been developed using a rigorous Koopmans approach, which has not been previously carried out for anatase TiO_2. Previous works have used a standard 25% of HF exact exchange through the HSE or B3LYP functionals,[64,101] while the DFT+U approach from other works has tailored a +U value to the experimental band gap that provides an underestimated band gap, and incomplete description of the electronic properties for anatase TiO_2.[67,71,72] The transfer-ability of the +U method is also contentious and if the band gap changes for surface states/properties then the selected value of +U is invalid. Since our value of HF exchange is Koopmans compliant, we are confident that the developed value from this approach is transferable to model the electronic properties of anatase TiO_2 surfaces without any constraints to the band gap or other electronic features of TiO_2.

Modelling the behaviour of excess electrons in the surfaces of anatase TiO_2 shows that the use of 25% HF exchange over binds the electron to the surface, resulting in a poor description of the electron trapping properties of the surfaces. Using our value of HF exchange (10.5%) we show that the perfect flat low index surfaces (001, 100, 101, 110, 112) do not have electron traps, preferring a delocalised solution across multiple Ti surface cations, in a similar manner to bulk anatase TiO_2. The higher index planes (103, 105, 107) of anatase TiO_2 do trap electrons at the lower coordinated Ti surface cations located at their surface defective steps. The presence of these four coordinated Ti cations introduces Ti $3d$ peaks at the bottom of the conduction band that are easily accessible and populated by excess electrons introduced into the surfaces. These features at the bottom of the conduction band for the stepped

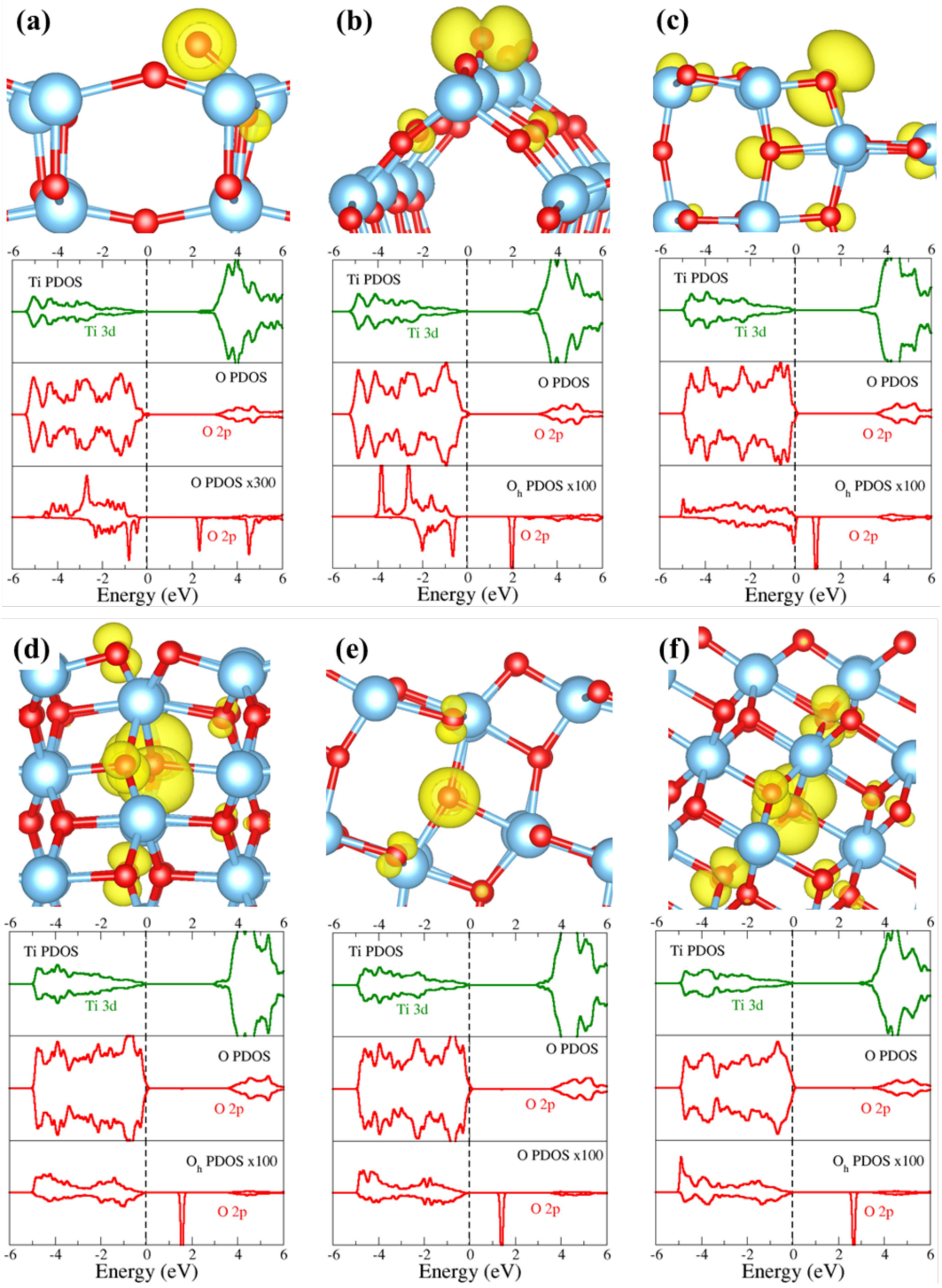

Figure 8: The local geometry (along the a-vector) and PDOS for holes trapped at the (a) 001, (b) 001-recon, (c) 100, (d) 101, (e) 110, and (f) 112, surfaces of anatase TiO_2. The yellow isosurface ($0.0015\,\text{electrons}/\text{a}_o{}^{-3}$) shows the location of the trapped hole polaron, while green and red lines are the Ti $3d$ and O $2p$ states, where the dotted black line indicates the position of the Fermi level.

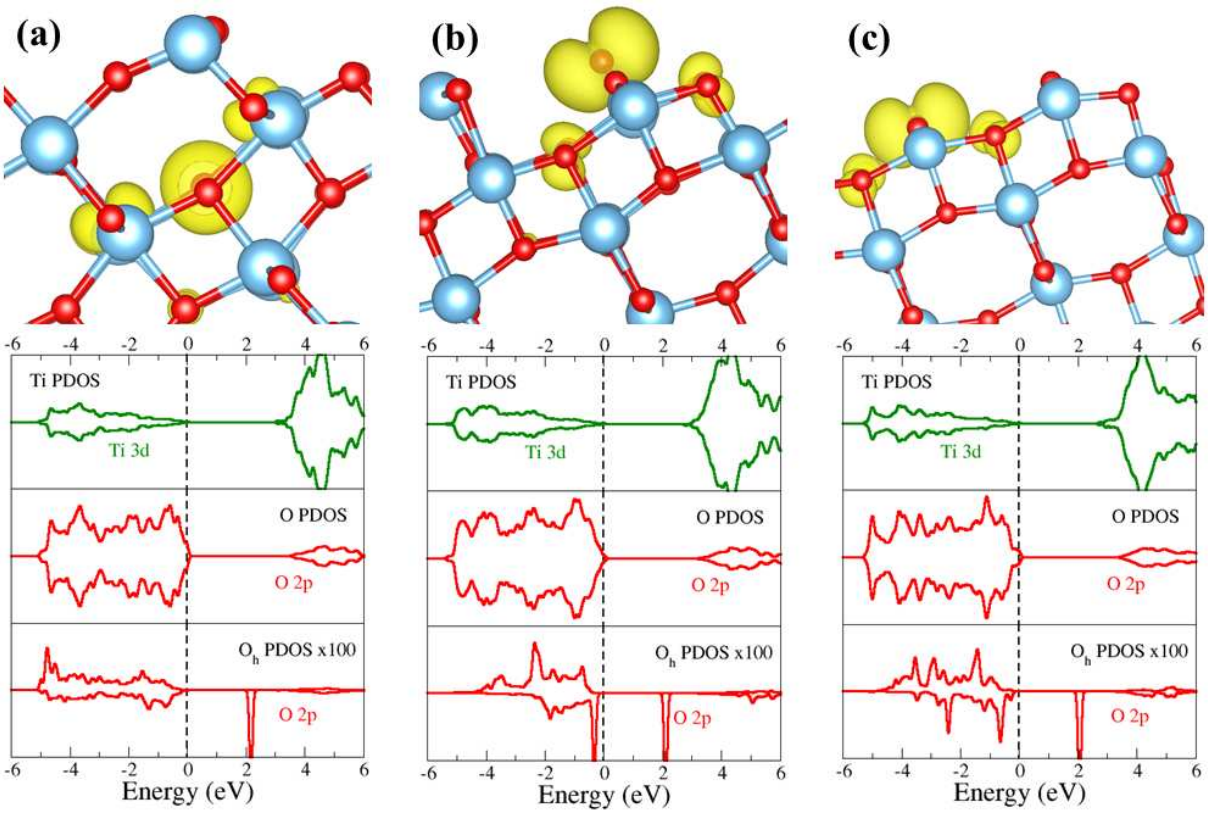

Figure 9: The local geometry (along the a-vector) and PDOS for holes trapped at the (a) 103, (b) 105, and (c) 107, high index surfaces of anatase TiO_2. The yellow iso-surface ($0.0015\,\text{electrons}/\text{a}_o{}^{-3}$) shows the location of the trapped hole polaron, while green and red lines are the Ti $3d$ and O $2p$ states, where the dotted black line indicates the position of the Fermi level.

surfaces are not seen on the low index planes or bulk TiO_2 which have a much broader Ti $3d$ band, thus resulting in no observable electron trapping. These results indicate that in order to minimize electron trapping when preparing anatase TiO_2 nano-crystals, the crystals must be maximized with low index planes without any higher index facets that will contain surface defects such as steps to intrinsically trap electrons.

The hole trapping capabilities for the low and high index anatase surfaces is found to be favoured across a distribution of sub-surface and surface sites. The strength of the surface hole trap is found to be facet dependent where the 001 and 105 surfaces show the strongest affinity to trap holes, and the 103/112 surfaces have the weakest hole trapping energies. The ability of the 001 surface to strongly trap holes by forming O^- surface species is vital for charge separation in photo-excited TiO_2 crystals and are useful for hole generation during photocatalysis. The 105 and 107 facets are also seen to have a strong hole trapping energy, where these defects could be present on 001 planes on anatase crystals since they have 001 terraces separated by steps. Similarly for the 100 surface, holes traps are present on the surface but are not as strongly trapped as the 001 surface. Both the 001 and 100 surfaces are seen experimentally on anatase TiO_2 nano-crystals and while the strong trapping of holes can be advantageous to photocatalysis, the presence of holes on these facets can be detrimental to electron mobility as any electrons close to these surfaces, donated from an external bias or molecular adsorbate will fill the hole and kill any conductivity.

Not only are the holes weakly trapping on the 101, 110, 112 and 103 surfaces, but the distribution of favoured hole trapping sites are all below the surface layers and disfavoured at the surface, indicating that holes are unlikely to be present on these surface planes. The presence of holes in the sub surface layers indicates that holes are not likely to be involved in catalysis on these facets, which is more likely on the 001 type-surfaces. Additionally, holes being more likely trapped in the sub-surface and not at the surface will allow longer lifetimes of any electrons present on these facets before recombination can take place. This is useful for charge separation of electrons and holes between the 001 and 101 surfaces, or useful in

catalysis where longer electron lifetimes on these facets can be beneficial for interacting with surface adsorbates.

Conclusion

Electron and hole polaron trapping was investigated on the low and high index surfaces of anatase TiO_2 using a hybrid density functional theory approach. Using an α value of 10.5% Hartree-Fock exact exchange that was previously developed for bulk anatase, we find that excess electron polarons do not intrinsically trap on the low index planes of anatase crystals which is a similar result to the bulk. For the higher index planes that contain structural step defects, we find that electrons do trap at the low coordinated Ti cations present at the steps. This has implications in photovoltaics as the presence of surface defects will trap electrons and reduce electron mobility and solar cell efficiency. For catalysis however, this may be beneficial for electron/hole charge separation, and they surplus of electrons may assist in surface mechanisms. The trapping of holes at the surfaces of anatase TiO_2 is a more complicated picture, as the distribution of hole traps is facet dependent. 001 and 100 surfaces, as well as 105 and 107 surfaces which have 001 type terraces, have the strongest affinity to trap holes at their facets which is important for charge separation on anatase crystals. The presence of holes on these surfaces is also expected to be vital to the photocatalytic properties of TiO_2 nanoparticles, as the holes can interact with molecular adsorbates. Hole trapping for the 101, 110, 112 and 103 surfaces is found to be favoured in the sub surface layers and not at the surface facet which can aid in longer lifetimes of electrons to prevent recombination. The calculated defect levels in the PDOS plots for electrons on the high index planes, and the holes on all surfaces can provide insight into UV and EPR experiments. The energy of the defect level can be compared to the experimental signal on the spectra and could provide guidance on the surface facet where the electron or hole is trapping; ie if the EPR signal is in a similar region to the defect level of the trapped

electron on the higher index 103 plane, then the theory can distinguish between the electron trapped at this plane and not by some point defect on the low index plane.

Supporting Information

The supporting information shows the Wulff construction for anatase TiO_2 nanoparticles from the calculated surface energies (Figure S1 (a)), the Wulff construction when there is a reduction in surface energies by 10% and 20% (Figure S1 (b)) and the change in atomic positions during relaxation (Figures S2-S4).

Acknowledgement

K.P.M. and J.J.C acknowledge support from EPSRC (EP/K003151/1, EP/P006051/1 and EP/P023843/1). This work made use of the facilities of Archer, the UK's national high-performance computing service, via our membership in the UK HPC Materials Chemistry Consortium, which is funded by EPSRC (EP/L000202/1). This work also made use of the facilities of N8 HPC Centre of Excellence, provided and funded by the N8 consortium and EPSRC (EP/K000225/1). The Centre is coordinated by the Universities of Leeds and Manchester. All data created during this research are available by request from the University of York Research database.

References

(1) Gordon, T. R.; Cargnello, M.; Paik, T.; Mangolini, F.; Weber, R.; Fornasiero, P.; Murray, C. Nonaqueous Synthesis of TiO_2 Nanocrystals Using TiF_4 to Engineer Morphology, Oxygen Vacancy Concentration, and Photocatalytic Activity. *Journal of the American Chemical Society* **2012**, *134*, 6751–6761.

(2) Jian, P.; Gang, L.; Qing, L. G.; Hui-Ming, C. On the True Photoreactivity Order

of {001}, {010}, and {101} Facets of Anatase TiO_2 Crystals. *Angewandte Chemie International Edition* **2011**, *50*, 2133–2137.

(3) Zheng, Z.; Huang, B.; Lu, J.; Qin, X.; Zhang, X.; Dai, Y. Hierarchical TiO_2 Microspheres: Synergetic Effect of {001} and {101} Facets for Enhanced Photocatalytic Activity. *Chemistry A European Journal* **2011**, *17*, 15032–15038.

(4) Wang, Z.; Huang, B.; Dai, Y.; Liu, Y.; Zhang, X.; Qin, X.; Wang, J.; Zheng, Z.; Cheng, H. Crystal Facets Controlled Synthesis of Graphene at TiO_2 Nanocomposites by a One-pot Hydrothermal Process. *CrystEngComm* **2012**, *14*, 1687–1692.

(5) Yang, H. G.; Sun, C. H.; Qiao, S. Z.; Zou, J.; Liu, G.; Smith, S. C.; Cheng, H. M.; Lu, G. Q. Anatase TiO_2 Single Crystals with a Large Percentage of Reactive Facets. *Nature* **2008**, *453*, 638–641.

(6) Etgar, L.; Zhang, W.; Gabriel, S.; Hickey, S. G.; Nazeeruddin, M. K.; Eychmüller, A.; Liu, B.; Grätzel, M. High Efficiency Quantum Dot Heterojunction Solar Cell Using Anatase (001) TiO_2 Nanosheets. *Advanced Materials* **2012**, *24*, 2202–2206.

(7) Nolan, M.; IwaszuK, A.; Lucid, A. K.; Carey, J. J.; Fronzi, M. Design of Novel Visible Light Active Photocatalyst Materials: Surface Modified TiO_2. *Advanced Materials* **2016**, *28*, 5425–5446.

(8) Kandavelu, V.; Kastien, H.; Thampi, K. R. Photocatalytic Degradation of Isothiazolin-3-ones in Water and Emulsion Paints Containing Nanocrystalline TiO_2 and ZnO Catalysts. *Applied Catalysis B: Environmental* **2004**, *48*, 101–111.

(9) Maggos, T.; Bartzis, J.; Liakou, M.; Gobin, C. Photocatalytic Degradation of NO_x Gases Using TiO_2-Containing Paint: A Real Scale Study. *Journal of hazardous materials* **2007**, *146*, 668–673.

(10) Ruiz, A. M.; Sakai, G.; Cornet, A.; Shimanoe, K.; Morante, J. R.; Yamazoe, N. Cr-doped TiO_2 Gas Sensor for Exhaust NO_2 Monitoring. *Sensors and Actuators B: Chemical* **2003**, *93*, 509–518.

(11) Ferroni, M.; Guidi, V.; Martinelli, G.; Faglia, G.; Nelli, P.; Sberveglieri, G. Characterization of a Nanosized TiO_2 Gas Sensor. *Nanostructured materials* **1996**, *7*, 709–718.

(12) Eranna, G.; Joshi, B.; Runthala, D.; Gupta, R. Oxide Materials for Development of Integrated Gas Sensors: A Comprehensive Review. *Critical Reviews in Solid State and Materials Sciences* **2004**, *29*, 111–188.

(13) Fateh, R.; Ismail, A. A.; Dillert, R.; Bahnemann, D. W. Highly Active Crystalline Mesoporous TiO_2 Films Coated onto Polycarbonate Substrates for Self-Cleaning Applications. *The Journal of Physical Chemistry C* **2011**, *115*, 10405–10411.

(14) Xi, B.; Verma, L. K.; Li, J.; Bhatia, C. S.; Danner, A. J.; Yang, H.; Zeng, H. C. TiO_2 Thin Films Prepared via Adsorptive Self-Assembly for Self-Cleaning Applications. *ACS Applied Materials & Interfaces* **2012**, *4*, 1093–1102.

(15) Esterkin, C.; Negro, A.; Alfano, O.; Cassano, A. Air Pollution Remediation in a Fixed Bed Photocatalytic Reactor Coated with TiO_2. *AIChE Journal* **2005**, *51*, 2298–2310.

(16) Antonello, A.; Soliveri, G.; Meroni, D.; Cappelletti, G.; Ardizzone, S. Photocatalytic Remediation of Indoor Pollution by Transparent TiO_2 Films. *Catalysis today* **2014**, *230*, 35–40.

(17) Fujishima, A.; Honda, K. Electrochemical Photolysis of Water at a Semiconductor Electrode. *Nature* **1972**, *238*, 37–38.

(18) Khan, S. U.; Al-Shahry, M.; Ingler, W. B. Efficient Photochemical Water Splitting by a Chemically Modified n-TiO_2. *Science* **2002**, *297*, 2243–2245.

(19) Ni, M.; Leung, M. K.; Leung, D. Y.; Sumathy, K. A Review and Recent Developments in Photocatalytic Water-Splitting Using TiO_2 for Hydrogen Production. *Renewable and Sustainable Energy Reviews* **2007**, *11*, 401–425.

(20) Rhatigan, S.; Nolan, M. CO_2 and Water Activation on Ceria Nanocluster Modified TiO_2 Rutile (110). *J. Mater. Chem. A* **2018**, *6*, 9139–9152.

(21) Fronzi, M.; Daly, W.; Nolan, M. Reactivity of Metal Oxide Nanocluster Modified Rutile and Anatase TiO_2: Oxygen Vacancy Formation and CO_2 Interaction. *Applied Catalysis A: General* **2016**, *521*, 240 – 249, SI:Photocatalysis.

(22) Yu, J.; Low, J.; Xiao, W.; Zhou, P.; Jaroniec, M. Enhanced Photocatalytic CO_2-Reduction Activity of Anatase TiO_2 by Coexposed {001} and {101} Facets. *Journal of the American Chemical Society* **2014**, *136*, 8839–8842.

(23) Ye, L.-H.; Freeman, A. J. Defect Compensation, Clustering, and Magnetism in Cr-doped Anatase TiO_2. *Phys. Rev. B* **2006**, *73*, 081304.

(24) Chen, J. S.; Tan, Y. L.; Li, C. M.; Cheah, Y. L.; Luan, D.; Madhavi, S.; Boey, F. Y. C.; Archer, L. A.; Lou, X. W. Constructing Hierarchical Spheres from Large Ultrathin Anatase TiO_2 Nanosheets with Nearly 100% Exposed (001) Facets for Fast Reversible Lithium Storage. *Journal of the American Chemical Society* **2010**, *132*, 6124–6130.

(25) Wang, Q.; Wen, Z.; Li, J. A Hybrid Supercapacitor Fabricated with a Carbon Nanotube Cathode and a TiO_2-B Nanowire Anode. *Advanced Functional Materials* **2006**, *16*, 2141–2146.

(26) Kang, T.-S.; Smith, A. P.; Taylor, B. E.; Durstock, M. F. Fabrication of Highly-Ordered TiO_2 Nanotube Arrays and Their Use in Dye-Sensitized Solar Cells. *Nano Letters* **2009**, *9*, 601–606.

(27) Kuang, D.; Brillet, J.; Chen, P.; Takata, M.; Uchida, S.; Miura, H.; Sumioka, K.; Zakeeruddin, S. M.; Grätzel, M. Application of Highly Ordered TiO_2 Nanotube Arrays in Flexible Dye-Sensitized Solar Cells. *ACS Nano* **2008**, *2*, 1113–1116.

(28) Fahmi, A.; Minot, C.; Silvi, B.; Causá, M. Theoretical Analysis of the Structures of Titanium Dioxide Crystals. *Phys. Rev. B* **1993**, *47*, 11717–11724.

(29) Fox, M. A.; Dulay, M. T. Heterogeneous Photocatalysis. *Chemical Reviews* **1993**, *93*, 341–357.

(30) Linsebigler, A. L.; Lu, G.; Yates, J. T. Photocatalysis on TiO_2 Surfaces: Principles, Mechanisms, and Selected Results. *Chemical Reviews* **1995**, *95*, 735–758.

(31) Naicker, P. K.; Cummings, P. T.; Zhang, H.; Banfield, J. F. Characterization of Titanium Dioxide Nanoparticles Using Molecular Dynamics Simulations. *The Journal of Physical Chemistry B* **2005**, *109*, 15243–15249, PMID: 16852930.

(32) Reddy, K. M.; Manorama, S. V.; Reddy, A. R. Bandgap Studies on Anatase Titanium Dioxide Nanoparticles. *Materials Chemistry and Physics* **2003**, *78*, 239 – 245.

(33) Sankapal, B.; Lux-Steiner, M.; Ennaoui, A. Synthesis and Characterization of Anatase-TiO_2 Thin Films. *Applied Surface Science* **2005**, *239*, 165 – 170.

(34) Tang, H.; Prasad, K.; Sanjinés, R.; Schmid, P. E.; Lévy, F. Electrical and Optical Properties of TiO_2 Anatase Thin Films. *Journal of Applied Physics* **1994**, *75*, 2042–2047.

(35) Richter, C.; Schmuttenmaer, C. A. Exciton-Like Trap States Limit Electron Mobility in TiO_2 Nanotubes. *Nature Nanotechnology* **2010**, *5*, 769772.

(36) Frölich, H. Electrons in Lattice Fields. *Advances in Physics* **1954**, *3*, 325–361.

(37) Austin, I. G.; Mott, N. F. Polarons in Crystalline and Non-Crystalline Materials. *Advances in Physics* **2001**, *50*, 757–812.

(38) Nakaoka, Y.; Nosaka, Y. ESR Investigation into the Effects of Heat Treatment and Crystal Structure on Radicals Produced over Irradiated TiO_2 Powder. *Journal of Photochemistry and Photobiology A: Chemistry* **1997**, *110*, 299–305.

(39) Dimitrijevic, N. M.; Saponjic, Z. V.; Rabatic, B. M.; Poluektov, O. G.; Rajh, T. Effect of Size and Shape of Nanocrystalline TiO_2 on Photogenerated Charges. An EPR Study. *The Journal of Physical Chemistry C* **2007**, *111*, 14597–14601.

(40) Coronado, J. M.; Maira, A. J.; Conesa, J. C.; Yeung, K. L.; Augugliaro, V.; Soria, J. EPR Study of the Surface Characteristics of Nanostructured TiO_2 Under UV Irradiation. *Langmuir* **2001**, *17*, 5368–5374.

(41) Micic, O. I.; Zhang, Y.; Cromack, K. R.; Trifunac, A. D.; Thurnauer, M. C. Trapped Holes on Titania Colloids Studied by Electron Paramagnetic Resonance. *The Journal of Physical Chemistry* **1993**, *97*, 7277–7283.

(42) Nosaka, Y.; Kishimoto, M.; Nishino, J. Factors Governing the Initial Process of TiO_2 Photocatalysis Studied by Means of In-situ Electron Spin Resonance Measurements. *The Journal of Physical Chemistry B* **1998**, *102*, 10279–10283.

(43) Tang, H.; Berger, H.; Schmid, P.; Levy, F. Optical Properties of Anatase (TiO_2). *Solid State Communications* **1994**, *92*, 267–271.

(44) Watanabe, M.; Hayashi, T. Time-Resolved Study of Self-trapped Exciton Luminescence in Anatase TiO_2 Under Two-photon Excitation. *Journal of luminescence* **2005**, *112*, 88–91.

(45) Cavigli, L.; Bogani, F.; Vinattieri, A.; Faso, V.; Baldi, G. Volume Versus Surface-Mediated Recombination in Anatase TiO_2 Nanoparticles. *Journal of Applied Physics* **2009**, *106*, 053516.

(46) Preclíková, J.; Galář, P.; Trojánek, F.; Daniš, S.; Rezek, B.; Gregora, I.; Němcová, Y.; Malỳ, P. Nanocrystalline Titanium Dioxide Films: Influence of Ambient Conditions on Surface and Volume Related Photoluminescence. *Journal of Applied Physics* **2010**, *108*, 113502.

(47) Thompson, T. L.; Yates, J. T. Monitoring Hole Trapping in Photoexcited TiO_2 (110) Using a Surface Photoreaction. *The Journal of Physical Chemistry B* **2005**, *109*, 18230–18236, PMID: 16853345.

(48) Roy, N.; Sohn, Y.; Pradhan, D. Synergy of Low Energy {101} and High Energy {001} TiO_2 Crystal Facets for Enhanced Photocatalysis. *ACS nano* **2013**, *7*, 2532–2540.

(49) Dinh, C.-T.; Nguyen, T.-D.; Kleitz, F.; Do, T.-O. Shape Controlled Synthesis of Highly Crystalline Titania Nanocrystals. *ACS nano* **2009**, *3*, 3737–3743.

(50) Wu, B.; Guo, C.; Zheng, N.; Xie, Z.; Stucky, G. D. Nonaqueous Production of Nanostructured Anatase with High-Energy Facets. *Journal of the American Chemical Society* **2008**, *130*, 17563–17567.

(51) Li, J.; Xu, D. Tetragonal Faceted Nanorods of Anatase TiO_2 Single Crystals with a Large Percentage of Active {100} Facets. *Chem. Commun.* **2010**, *46*, 2301–2303.

(52) Liu, G.; Sun, C.; Yang, H. G.; Smith, S. C.; Wang, L.; Lu, G. Q.; Cheng, H.-M. Nanosized Anatase TiO_2 Single Crystals for Enhanced Photocatalytic Activity. *Chem. Commun.* **2010**, *46*, 755–757.

(53) Selloni, A. Crystal Growth: Anatase Shows its Reactive Side. *Nature* **2008**, *7*, 613–615.

(54) Lazzeri, M.; Vittadini, A.; Selloni, A. Structure and Energetics of Stoichiometric TiO_2 Anatase Surfaces. *Phys. Rev. B* **2001**, *63*, 155409.

(55) Fang, W. Q.; Gong, X.-Q.; Yang, H. G. On the Unusual Properties of Anatase TiO_2 Exposed by Highly Reactive Facets. *The Journal of Physical Chemistry Letters* **2011**, *2*, 725–734.

(56) Murakami, N.; Kurihara, Y.; Tsubota, T.; Ohno, T. Shape-Controlled Anatase Titanium(IV) Oxide Particles Prepared by Hydrothermal Treatment of Peroxo Titanic Acid in the Presence of Polyvinyl Alcohol. *The Journal of Physical Chemistry C* **2009**, *113*, 3062–3069.

(57) Maitani, M. M.; Tanaka, K.; Mochizuki, D.; Wada, Y. Enhancement of Photoexcited Charge Transfer by {001} Facet-Dominating TiO_2 Nanoparticles. *The Journal of Physical Chemistry Letters* **2011**, *2*, 2655–2659.

(58) Chang, L.; Xiguang, H.; Shuifen, X.; Qin, K.; Xue, W.; Mingshang, J.; Zhaoxiong, X.; Lansun, Z. Enhancing the Photocatalytic Activity of Anatase TiO_2 by Improving the Specific Facet-Induced Spontaneous Separation of Photogenerated Electrons and Holes. *Chemistry An Asian Journal* **2012**, *8*, 282–289.

(59) Wu, N.; Wang, J.; Tafen, D. N.; Wang, H.; Zheng, J.-G.; Lewis, J. P.; Liu, X.; Leonard, S. S.; Manivannan, A. Shape-Enhanced Photocatalytic Activity of Single-Crystalline Anatase TiO_2 (101) Nanobelts. *Journal of the American Chemical Society* **2010**, *132*, 6679–6685.

(60) Giocondi, J. L.; Salvador, P. A.; Rohrer, G. S. The Origin of Photochemical Anisotropy in $SrTiO_3$. *Topics in Catalysis* **2007**, *44*, 529–533.

(61) Tachikawa, T.; Yamashita, S.; Majima, T. Evidence for Crystal-Face-Dependent TiO_2 Photocatalysis from Single-Molecule Imaging and Kinetic Analysis. *Journal of the American Chemical Society* **2011**, *133*, 7197–7204.

(62) Cococcioni, M.; de Gironcoli, S. Linear Response Approach to the Calculation of the

Effective Interaction Parameters in the LDA + U Method. *Phys. Rev. B* **2005**, *71*, 035105.

(63) Mori-Sánchez, P.; Cohen, A. J.; Yang, W. Localization and Delocalization Errors in Density Functional Theory and Implications for Band-Gap Prediction. *Phys. Rev. Lett.* **2008**, *100*, 146401.

(64) Finazzi, E.; Di Valentin, C.; Pacchioni, G.; Selloni, A. Excess Electron States in Reduced Bulk Anatase TiO_2: Comparison of Standard GGA, GGA+U, and Hybrid DFT Calculations. *The Journal of Chemical Physics* **2008**, *129*, 154113.

(65) Na-Phattalung, S.; Smith, M. F.; Kim, K.; Du, M.-H.; Wei, S.-H.; Zhang, S. B.; Limpijumnong, S. First-Principles Study of Native Defects in Anatase TiO_2. *Phys. Rev. B* **2006**, *73*, 125205.

(66) Di Valentin, C.; Pacchioni, G.; Selloni, A. Electronic Structure of Defect States in Hydroxylated and Reduced Rutile TiO_2(110) Surfaces. *Phys. Rev. Lett.* **2006**, *97*, 166803.

(67) Morgan, B. J.; Watson, G. W. A DFT+U Description of Oxygen Vacancies at the TiO_2 Rutile (110) Surface. *Surface Science* **2007**, *601*, 5034 – 5041.

(68) Calzado, C. J.; Hernández, N. C.; Sanz, J. F. Effect of On-Site Coulomb Repulsion Term U on the Band-Gap States of the Reduced Rutile (110) TiO_2 Surface. *Phys. Rev. B* **2008**, *77*, 045118.

(69) Morgan, B. J.; Watson, G. W. Polaronic Trapping of Electrons and Holes by Native Defects in Anatase TiO_2. *Phys. Rev. B* **2009**, *80*, 233102.

(70) Morgan, B. J.; Watson, G. W. Intrinsic N-type Defect Formation in TiO_2: A Comparison of Rutile and Anatase from GGA+U Calculations. *The Journal of Physical Chemistry C* **2010**, *114*, 2321–2328.

(71) Deskins, N. A.; Dupuis, M. Electron Transport via Polaron Hopping in Bulk TiO_2: A Density Functional Theory Characterization. *Phys. Rev. B* **2007**, *75*, 195212.

(72) Deskins, N. A.; Dupuis, M. Intrinsic Hole Migration Rates in TiO_2 from Density Functional Theory. *The Journal of Physical Chemistry C* **2009**, *113*, 346–358.

(73) Morgan, B. J.; Scanlon, D. O.; Watson, G. W. Small Polarons in Nb- and Ta- Doped Rutile and Anatase TiO_2. *J. Mater. Chem.* **2009**, *19*, 5175–5178.

(74) Mulmi, D. D.; Sekiya, T.; Kamiya, N.; Kurita, S.; Murakami, Y.; Kodaira, T. Optical and Electric Properties of Nb-doped Anatase TiO_2 Single Crystal. *Journal of Physics and Chemistry of Solids* **2004**, *65*, 1181 – 1185.

(75) Furubayashi, Y.; Hitosugi, T.; Yamamoto, Y.; Inaba, K.; Kinoda, G.; Hirose, Y.; Shimada, T.; Hasegawa, T. A Transparent Metal: Nb-doped Anatase TiO_2. *Applied Physics Letters* **2005**, *86*, 252101.

(76) Di Valentin, C.; Selloni, A. Bulk and Surface Polarons in Photoexcited Anatase TiO_2. *The Journal of Physical Chemistry Letters* **2011**, *2*, 2223–2228.

(77) Meriaudeau, P.; Che, M.; Jøorgensen, C. Angular Overlap Treatment and Electron Spin Resonance of Titanium(III) in Anatase. *Chemical Physics Letters* **1970**, *5*, 131 – 133.

(78) Wallace, S. K.; Mckenna, K. P. Facet-Dependent Electron Trapping in TiO_2 Nanocrystals. *The Journal of Physical Chemistry C* **2015**, *119*, 1913–1920.

(79) Deskins, N. A.; Rousseau, R.; Dupuis, M. Localized Electronic States from Surface Hydroxyls and Polarons in TiO_2 (110). *The Journal of Physical Chemistry C* **2009**, *113*, 14583–14586.

(80) Morgan, B. J.; Watson, G. W. A Density Functional Theory + U Study of Oxygen

Vacancy Formation at the (110), (100), (101), and (001) Surfaces of Rutile TiO_2. *The Journal of Physical Chemistry C* **2009**, *113*, 7322–7328.

(81) Deák, P.; Kullgren, J.; Frauenheim, T. Polarons and Oxygen Vacancies at the Surface of Anatase TiO_2. *physica status solidi (RRL)–Rapid Research Letters* **2014**, *8*, 583–586.

(82) Setvin, M.; Franchini, C.; Hao, X.; Schmid, M.; Janotti, A.; Kaltak, M.; Van de Walle, C. G.; Kresse, G.; Diebold, U. Direct View at Excess Electrons in TiO_2 Rutile and Anatase. *Phys. Rev. Lett.* **2014**, *113*, 086402.

(83) Moser, S.; Moreschini, L.; Jaćimović, J.; Barišić, O. S.; Berger, H.; Magrez, A.; Chang, Y. J.; Kim, K. S.; Bostwick, A.; Rotenberg, E.; Forró, L.; Grioni, M. Tunable Polaronic Conduction in Anatase TiO_2. *Phys. Rev. Lett.* **2013**, *110*, 196403.

(84) Jaćimović, J.; Vaju, C.; Magrez, A.; Berger, H.; Forró, L.; Gaal, R.; Cerovski, V.; Žikić, R. Pressure Dependence of the Large-Polaron Transport in Anatase TiO_2 Single Crystals. *EPL (Europhysics Letters)* **2012**, *99*, 57005.

(85) Elmaslmane, A. R.; Watkins, M. B.; McKenna, K. P. First-Principles Modeling of Polaron Formation in TiO_2 Polymorphs. *Journal of Chemical Theory and Computation* **2018**, *14*, 37403751.

(86) Guidon, M.; Hutter, J.; VandeVondele, J. Robust Periodic HartreeFock Exchange for Large-Scale Simulations Using Gaussian Basis Sets. *Journal of Chemical Theory and Computation* **2009**, *5*, 3010–3021.

(87) VandeVondele, J.; Krack, M.; Mohamed, F.; Parrinello, M.; Chassaing, T.; Hutter, J. Quickstep: Fast and Accurate Density Functional Calculations Using a Mixed Gaussian and Plane Waves Approach. *Computer Physics Communications* **2005**, *167*, 103 – 128.

(88) VandeVondele, J.; Hutter, J. Gaussian Basis Sets for Accurate Calculations on Molecular Systems in Gas and Condensed Phases. *The Journal of Chemical Physics* **2007**, *127*, 114105.

(89) Goedecker, S.; Teter, M.; Hutter, J. Separable Sual-Space Gaussian Pseudopotentials. *Phys. Rev. B* **1996**, *54*, 1703–1710.

(90) Hartwigsen, C.; Goedecker, S.; Hutter, J. Relativistic Separable Dual-Space Gaussian Pseudopotentials from H to Rn. *Phys. Rev. B* **1998**, *58*, 3641–3662.

(91) Krack, M. Pseudopotentials for H to Kr Optimized for Gradient-Corrected Exchange-Correlation Functionals. *Theoretical Chemistry Accounts* **2005**, *114*, 145–152.

(92) Murakami, M.; Matsumoto, Y.; Nakajima, K.; Makino, T.; Segawa, Y.; Chikyow, T.; Ahmet, P.; Kawasaki, M.; Koinuma, H. Anatase TiO_2 Thin Films Grown on Lattice-Matched $LaAlO_3$ Substrate by Laser Molecular-Beam Epitaxy. *Applied Physics Letters* **2001**, *78*, 2664–2666.

(93) Guidon, M.; Hutter, J.; VandeVondele, J. Auxiliary Density Matrix Methods for HartreeFock Exchange Calculations. *Journal of Chemical Theory and Computation* **2010**, *6*, 2348–2364.

(94) Watson, G. W.; Kelsey, E. T.; de Leeuw, N. H.; Harris, D. J.; Parker, S. C. Atomistic Simulation of Dislocations, Surfaces and Interfaces in MgO. *J. Chem. Soc., Faraday Trans.* **1996**, *92*, 433–438.

(95) Liang, Y.; Gan, S.; Chambers, S. A.; Altman, E. I. Surface Structure of Anatase $TiO_2(001)$: Reconstruction, Atomic Steps, and Domains. *Phys. Rev. B* **2001**, *63*, 235402.

(96) Xue-Qing Gong, M. B., Annabella Selloni; Diebold, U. Steps on anatase $TiO_2(101)$. *Nature Materials* **2006**, *5*, 665670.

(97) Joos, B.; Duesbery, M. The Peierls Stress of Dislocations: An Analytic Formula. *Physical Review Letters* **1997**, *78*, 266.

(98) Nabarro, F. Theoretical and Experimental Estimates of the Peierls Stress. *Philosophical Magazine A* **1997**, *75*, 703–711.

(99) Suzuki, K.; Ichihara, M.; Takeuchi, S. High-Resolution Electron Microscopy of Lattice Defects in TiO_2 and SnO_2. *Philosophical Magazine A* **1991**, *63*, 657–665.

(100) Takeuchi, S.; Hashimoto, T. Deformation Mechanisms in Titanium Dioxide Single Crystals. *Journal of Materials Science* **1990**, *25*, 417–423.

(101) Deák, P.; Aradi, B.; Frauenheim, T. Polaronic Effects in TiO_2 Calculated by the HSE06 Hybrid Functional: Dopant Passivation by Carrier Self Trapping. *Physical Review B* **2011**, *83*, 155207.

(102) Gono, P.; Wiktor, J.; Ambrosio, F.; Pasquarello, A. Surface Polarons Reducing Overpotentials in the Oxygen Evolution Reaction. *ACS Catalysis* **2018**, *8*, 5847–5851.

(103) Chen, S.; Wang, L. W. Double Hole Induced Oxygen Dimerization in Transition Metal Oxides. *Phys. Rev. B* **2014**, *89*, 014109.

Graphical TOC Entry

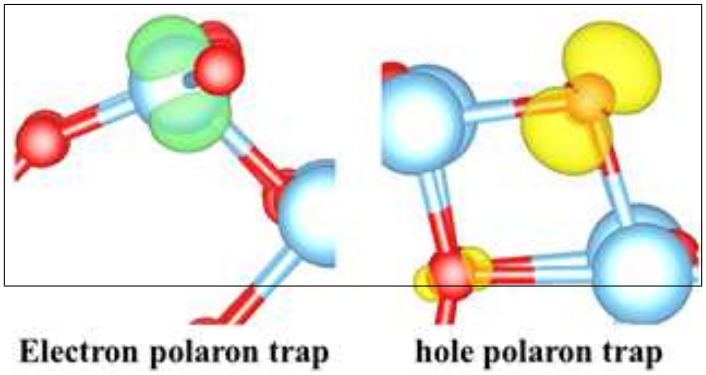

Supporting Information for the Article "Does Polaronic Self-Trapping Occur at Anatase TiO_2 Surfaces?"

John Carey and Keith McKenna

Physics Department, University of York, Heslington, York, YO10 5DD, United Kingdom

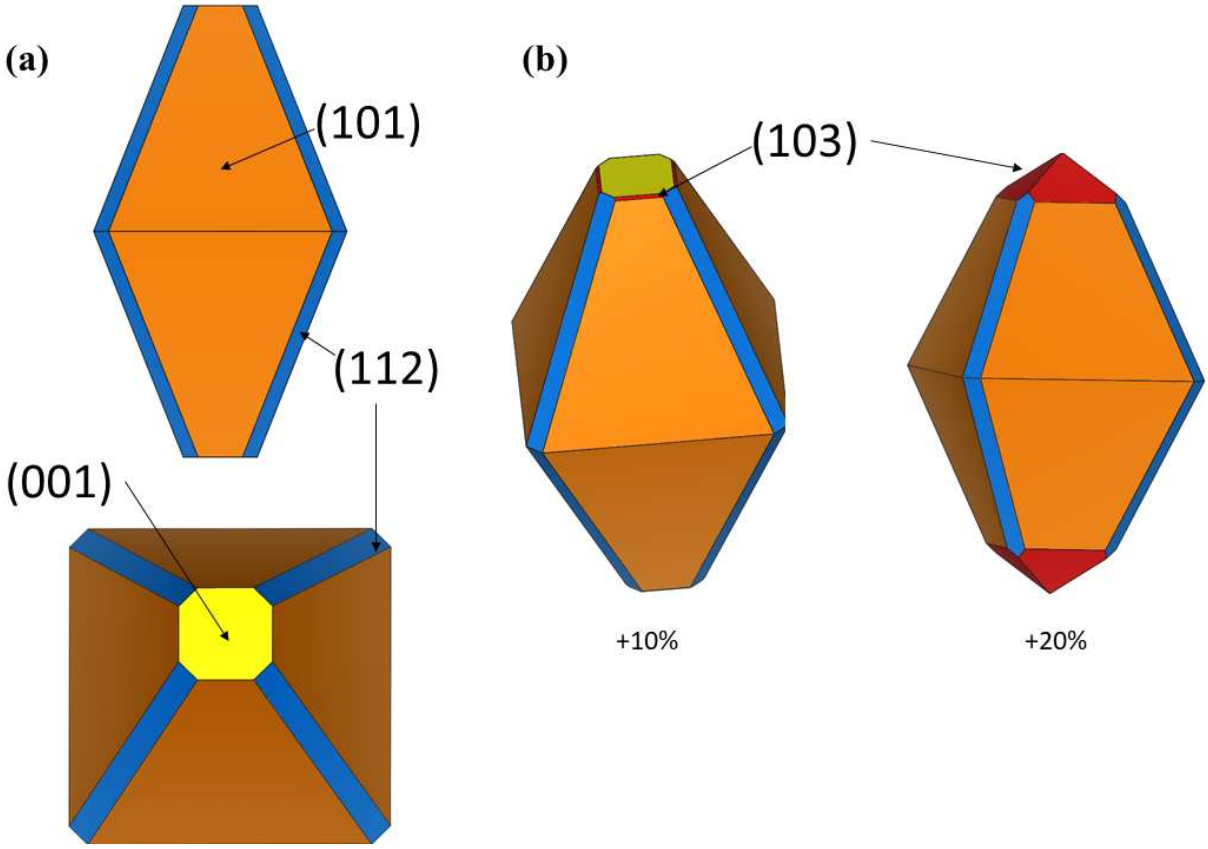

Figure S1: (a) The Wulff construction for the anatase TiO2 nano-particles using the DFT calculated surface energies, and (b) the Wulff construction when there is a reduction in the surface energies. The orange, yellow, blue and red areas are the 101, 001, 112 and 103 surfaces.

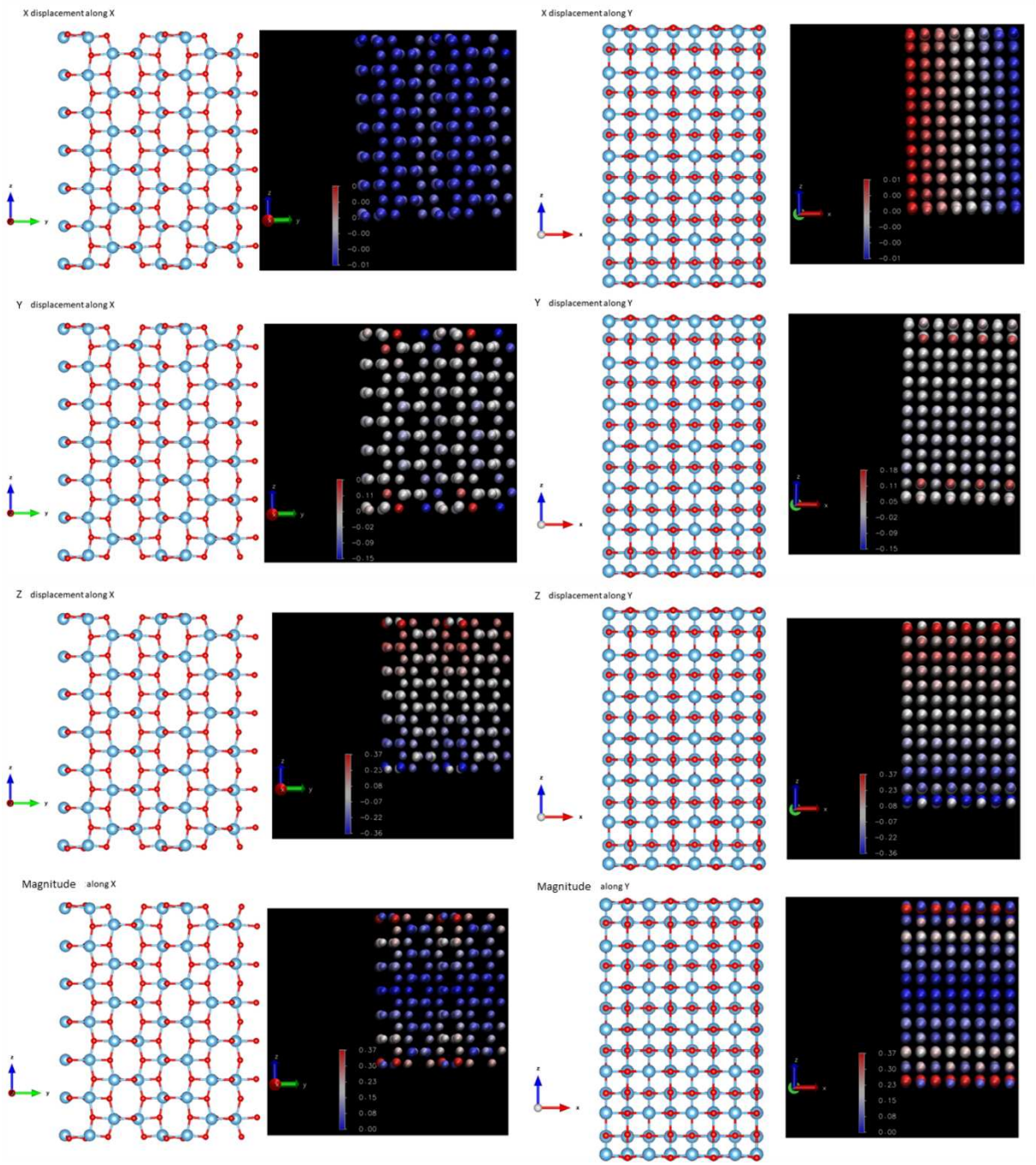

Figure S2: The ion relaxation in the 100 surface slab along the X and Y directions. The red and blue colours signify positive and negative changes as shown by the scales.

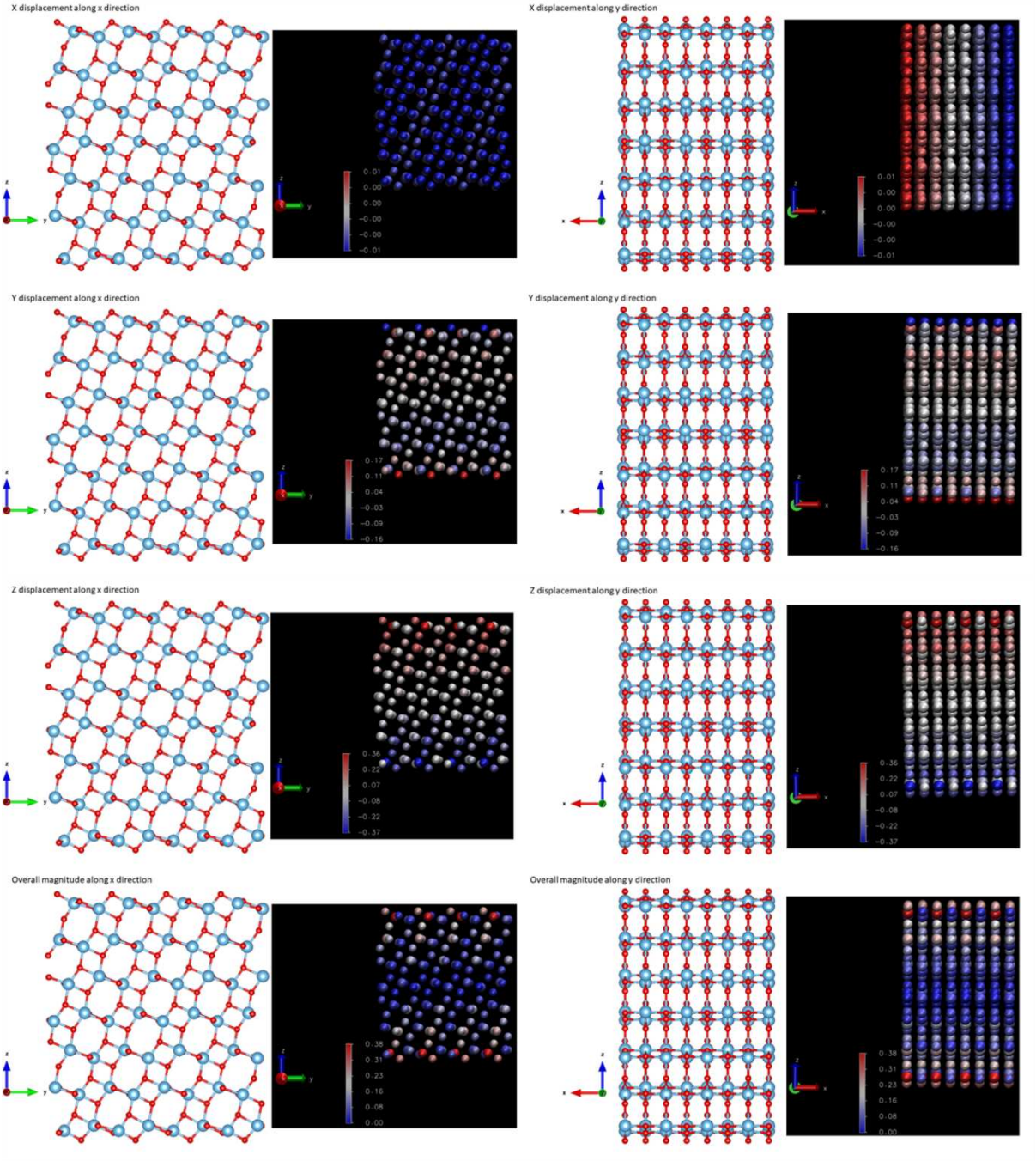

Figure S3:The ion relaxation in the 101 surface slab along the X and Y directions. The red and blue colours signify positive and negative changes as shown by the scales.

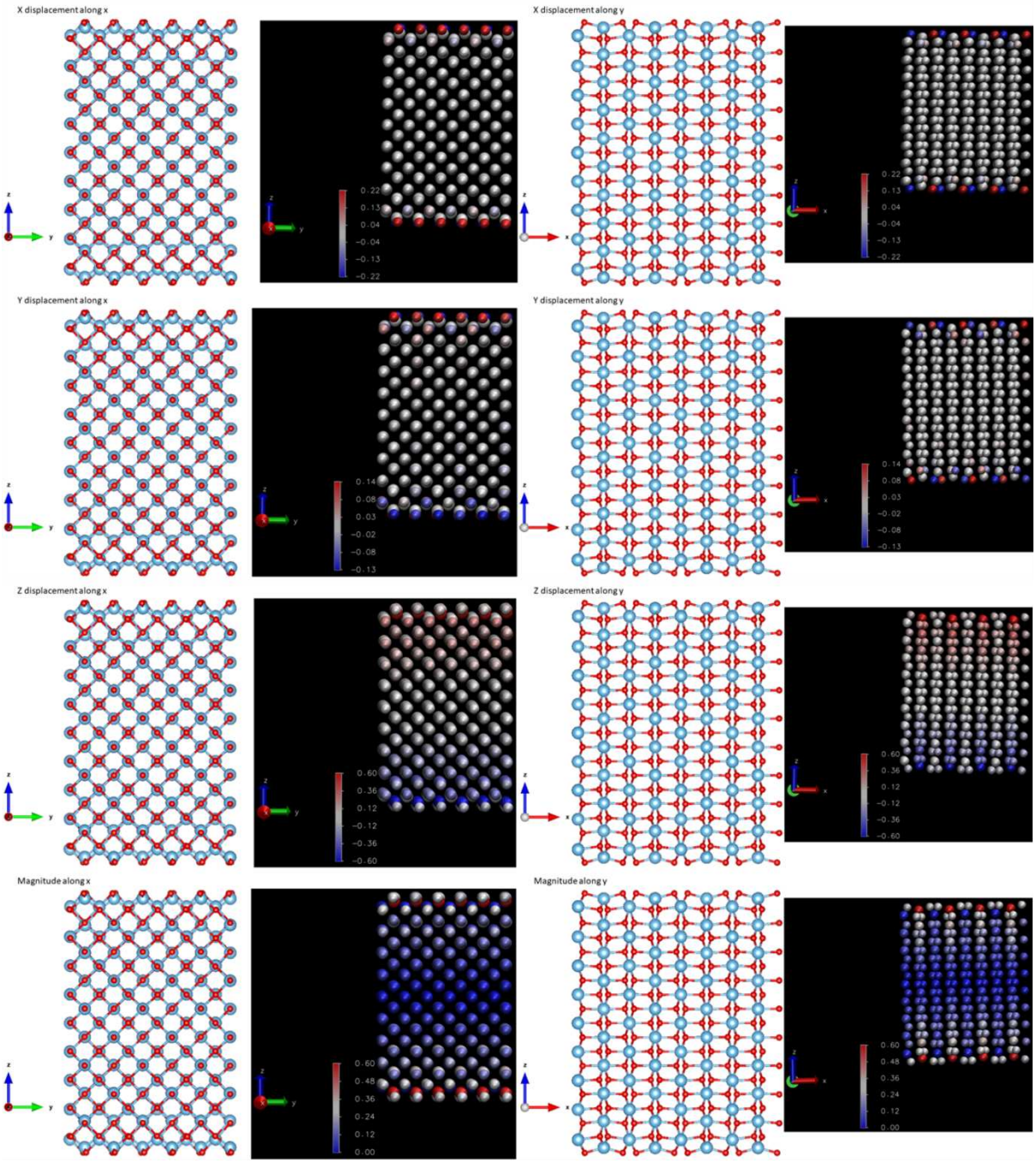

Figure S4: The ion relaxation in the 110 surface slab along the X and Y directions. The red and blue colours signify positive and negative changes as shown by the scales.